Supramolecular Structural Constraints on Alzheimer's β-Amyloid Fibrils from Electron Microscopy and Solid-State Nuclear Magnetic Resonance†

Oleg N. Antzutkin,‡ Richard D. Leapman,§ John J. Balbach,|| and Robert Tycko*,||

Division of Chemistry, Luleå University of Technology, Luleå, Sweden S-97187, Division of Bioengineering and Physical Science, Office of Research Services, National Institutes of Health, Bethesda, Maryland 20892-5766, and Laboratory of Chemical Physics, National Institute of Diabetes and Digestive and Kidney Diseases, National Institutes of Health, Bethesda, Maryland 20892-0520

Received June 14, 2002; Revised Manuscript Received October 15, 2002

ABSTRACT: We describe electron microscopy (EM), scanning transmission electron microscopy (STEM), and solid-state nuclear magnetic resonance (NMR) measurements on amyloid fibrils formed by the 42-residue β-amyloid peptide associated with Alzheimer's disease ($A\beta_{1-42}$) and by residues 10−35 of the full-length peptide ($A\beta_{10-35}$). These measurements place constraints on the supramolecular structure of the amyloid fibrils, especially the type of β-sheets present in the characteristic amyloid cross-β structural motif and the assembly of these β-sheets into a fibril. EM images of negatively stained $A\beta_{10-35}$ fibrils and measurements of fibril mass per length (MPL) by STEM show a strong dependence of fibril morphology and MPL on pH. $A\beta_{10-35}$ fibrils formed at pH 3.7 are single "protofilaments" with MPL equal to twice the value expected for a single cross-β layer. $A\beta_{10-35}$ fibrils formed at pH 7.4 are apparently pairs of protofilaments or higher order bundles. EM and STEM data for $A\beta_{1-42}$ fibrils indicate that protofilaments with MPL equal to twice the value expected for a single cross-β layer are also formed by $A\beta_{1-42}$ and that these protofilaments exist singly and in pairs at pH 7.4. Solid-state NMR measurements of intermolecular distances in $A\beta_{10-35}$ fibrils, using multiple-quantum ^{13}C NMR, $^{13}C-^{13}C$ dipolar recoupling, and $^{15}N-^{13}C$ dipolar recoupling techniques, support the in-register parallel β-sheet organization previously established by Lynn, Meredith, Botto, and co-workers [Benzinger et al. (1998) *Proc. Natl. Acad. Sci. U.S.A. 95*, 13407−13412; Benzinger et al. (2000) *Biochemistry 39*, 3491−3499] and show that this β-sheet organization is present at pH 3.7 as well as pH 7.4 despite the differences in fibril morphology and MPL. Solid-state NMR measurements of intermolecular distances in $A\beta_{1-42}$ fibrils, which represent the first NMR data on $A\beta_{1-42}$ fibrils, also indicate an in-register parallel β-sheet organization. These results, along with previously reported data on $A\beta_{1-40}$ fibrils, suggest that the supramolecular structures of $A\beta_{10-35}$, $A\beta_{1-40}$, and $A\beta_{1-42}$ fibrils are quite similar. A schematic structural model of these fibrils, consistent with known experimental EM, STEM, and solid-state NMR data, is presented.

Amyloid fibrils are filamentous structures formed by a variety of peptides and proteins with disparate lengths and amino acid sequences but sharing certain morphological, tinctorial, and molecular structural features (*1*). Interest in amyloid fibrils from the biomedical perspective stems from their involvement in amyloid diseases, including Alzheimer's disease, type 2 diabetes, Parkinson's disease, Huntington's disease, and transmissible spongiform encephalopathies (*2*). Amyloid fibrils associated with Alzheimer's disease are formed in vivo by the β-amyloid peptide ($A\beta$),[1] a peptide with length ranging from 39 to 43 residues due to variations in the C-terminal cleavage site (*3*−*5*). Additional interest from the perspectives of biophysical chemistry and structural biology stems from the recent realization that the amyloid fibril is a stable state of many, perhaps most, polypeptides under appropriate conditions, including polypeptides that have stable globular structures as monomers or multimers and are not associated with known amyloid diseases (*6*, *7*).

At the resolution of electron microscope (EM) images, amyloid fibrils formed by different polypeptides are remarkably similar, generally appearing as unbranched filaments with diameters of 5−10 nm and lengths exceeding 1 μm.

† O.N.A. is supported by a fellowship from the Swedish Foundation for International Cooperation in Research and Higher Education and a grant from the Swedish Natural Science Research Council.

* Corresponding author. Mailing address: National Institutes of Health, Building 5, Room 112, Bethesda, MD 20892-0520. Telephone: 301-402-8272. Fax: 301-496-0825. E-mail: tycko@helix.nih.gov.

‡ Luleå University of Technology.

§ Division of Bioengineering and Physical Science, Office of Research Services, National Institutes of Health.

|| Laboratory of Chemical Physics, National Institute of Diabetes and Digestive and Kidney Diseases, National Institutes of Health.

[1] Abbreviations: $A\beta$, β-amyloid; EM, electron microscope; NMR, nuclear magnetic resonance; $A\beta_{m-n}$, residues *m* through *n* of the full-length β-amyloid peptide; MQ, multiple quantum; MPL, mass per length; STEM, scanning transmission electron microscope; 1D, one dimensional; FMOC, fluorenylmethoxycarbonyl; TFA, trifluoroacetic acid; TBME, *tert*-butyl methyl ether; HPLC, high-performance liquid chromatography; TMV, tobacco mosaic virus; MAS, magic angle spinning; TMS, tetramethylsilane; rf, radio frequency; fpRFDR-CT, constant-time finite-pulse radio frequency-driven recoupling; REDOR, rotational echo double resonance; PSL, pulsed spin locking; AFM, atomic force microscope; fwhm, full width at half-maximum; DRAWS, dipolar recoupling with a windowless sequence; SANS, small angle neutron scattering; PEG, poly(ethylene glycol).

10.1021/bi0204185 CCC: $22.00
Published on Web 12/03/2002

Until recently, direct structural information at higher resolution has been scarce because of the inherent insoluble and noncrystalline nature of these materials. X-ray diffraction data on unaligned fibrils and aligned fibril bundles (*8*, *9*) have shown that a principal and defining molecular structural feature of all amyloid fibrils is the presence of β-sheets spanning the length of the fibril that are formed by β-strand segments that run approximately perpendicular to the long axis of the fibril and are connected by intermolecular hydrogen bonds approximately parallel to the long axis. This orientation of β-sheets is commonly called a cross-β structure.

Recent experiments by Lansbury, Griffin, and co-workers (*10*−*12*), by Lynn, Meredith, Botto, and co-workers (*13*−*16*), and by us (*17*−*21*) have demonstrated that important molecular level structural constraints on amyloid fibrils can be obtained from solid-state nuclear magnetic resonance (NMR) measurements. These measurements require neither crystallinity nor solubility. With appropriate isotopic (e.g., ^{13}C or ^{15}N) labeling, solid-state NMR techniques provide quantitative constraints on the supramolecular organization of β-sheets in amyloid fibrils (*11*, *13*−*18*, *20*) and on the torsion angles and interatomic distances that define the peptide conformation in a fibril (*11*, *12*, *14*, *16*, *18*, *21*). Solid-state NMR measurements also permit the characterization of the degree of structural order in amyloid fibrils and have demonstrated that amyloid fibrils contain regions in which both side chain and backbone atoms have nearly crystalline order (*18*, *21*, *22*).

An important result from solid-state NMR, originally reported by Lynn, Meredith, Botto, and co-workers (*13*), was the discovery that β-sheets in fibrils formed by residues 10−35 of Aβ (i.e., Aβ_{10-35}) have an in-register *parallel* organization, rather than the *antiparallel* organization indicated for Aβ fibrils by earlier infrared spectroscopic data (*23*−*25*) and incorporated into structural models of Aβ fibrils (*26*−*30*). This result was extended by Antzutkin et al. to fibrils formed by the full-length 40-residue β-amyloid peptide (Aβ_{1-40}), which were also found to have an in-register parallel organization of β-sheets by multiple-quantum (MQ) solid-state NMR (*17*, *31*) and by ^{13}C−^{13}C dipolar recoupling measurements (*20*). In contrast, Lansbury, Griffin, and co-workers found that fibrils formed by residues 34−42 of the 42-residue form of Aβ (Aβ_{34-42}) contain antiparallel β-sheets (*11*), and Balbach et al. found that fibrils formed by residues 16−22 (Aβ_{16-22}) also contain antiparallel β-sheets (*18*). Taken together, these solid-state NMR data on Aβ fibrils demonstrate that the supramolecular organization of amyloid fibrils is not universal and is not uniquely determined at the level of short (e.g., seven-residue) peptide segments.

This paper presents additional constraints on the supramolecular structure of amyloid fibrils formed by Aβ_{10-35} and by the 42-residue variant of full-length Aβ (Aβ_{1-42}), obtained from both EM and solid-state NMR measurements, including the first solid-state NMR data on Aβ_{1-42} fibrils. Figure 1 shows the sequences of the peptides Aβ_{10-35}, A$\beta_{10-35,Scr}$, and Aβ_{1-42} examined in this work. Aβ_{1-42} is the form of Aβ that is normally present at the second highest concentrations (after Aβ_{1-40}) in humans. Aβ_{1-42} has been shown to be the primary component of immature amyloid plaques (*32*, *33*). Genetic mutations associated with a predisposition toward Alzheimer's disease result in elevated Aβ_{1-42} levels (*34*). In vitro, Aβ_{1-42} has been shown to fibrillize more rapidly and at lower concentrations than Aβ_{1-40} (*35*, *36*). It has been unclear whether the properties of Aβ_{1-42} reflect distinct structural features of Aβ_{1-42} fibrils, relative to Aβ_{1-40} and Aβ_{10-35} fibrils, especially in light of the antiparallel β-sheet organization determined for Aβ_{34-42} (*11*).

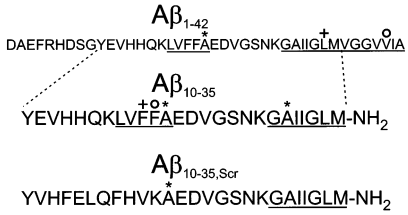

FIGURE 1: Amino acid sequences of the three β-amyloid peptides studied by electron microscopy and solid-state NMR techniques. Central and C-terminal hydrophobic segments are underlined. Symbols indicate residues that are labeled with ^{13}C at a methyl carbon (*), ^{13}C at a carbonyl carbon (+), or ^{15}N at an amide nitrogen (○) for solid-state NMR measurements.

Aβ_{10-35} is a model system for studies of Aβ fibrils (*37*−*39*) with the important features that it retains the central hydrophobic segment (residues 17−21) and a portion of the C-terminal hydrophobic segment (residues 29−35) of Aβ_{1-40} and Aβ_{1-42}. The first 10−12 residues at the N-terminus of full-length Aβ are known to be susceptible to proteolytic cleavage (*40*−*43*), and solid-state NMR measurements indicate that the N-terminal residues are disordered in Aβ_{1-40} fibrils (*17*, *20*, *21*). It therefore appears likely that the N-terminal residues deleted in Aβ_{10-35} do not play an important structural role in the amyloid fibrils. A$\beta_{10-35,Scr}$ has the same amino acid composition as Aβ_{10-35}, but the sequence of residues 11−20 is "scrambled" so that there are no contiguous hydrophobic residues. The hydrophobic segment spanning residues 17−21 has been shown to be important for fibrillization of Aβ_{10-35} (*38*), Aβ_{1-42} (*44*), and other Aβ peptides (*45*). This hydrophobic segment is destroyed in A$\beta_{10-35,Scr}$, while the C-terminal hydrophobic segment is preserved. A$\beta_{10-35,Scr}$ serves as a control for EM and solid-state NMR measurements.

Data presented in this paper include (1) EM images of Aβ_{10-35} that demonstrate a strong dependence of fibril morphology on pH, (2) measurements of the mass per length (MPL) of Aβ_{10-35} fibrils by scanning transmission electron microscopy (STEM) that suggest the existence of a protofilament constructed from two cross-β units (see Results for definitions of these terms), (3) EM images and MPL measurements on Aβ_{1-42} fibrils that also suggest a protofilament constructed from two cross-β units, (4) one-dimensional (1D) solid-state ^{13}C NMR spectra of Aβ_{10-35} and Aβ_{1-42} fibrils with ^{13}C labels at specific sites, demonstrating characteristic changes in ^{13}C NMR line shapes that result from amyloid fibrillization and correlate with fibril morphology and MPL, (5) MQ, ^{13}C−^{13}C dipolar recoupling, and ^{15}N−^{13}C dipolar recoupling solid-state NMR measurements on Aβ_{10-35} fibrils that support an in-register parallel organization of β-sheets formed by the central and C-terminal hydrophobic segments, and (6) ^{13}C−^{13}C and ^{15}N−^{13}C dipolar recoupling measurements on Aβ_{1-42} fibrils that support a parallel organization of β-sheets and demonstrate that the antiparallel β-sheet structure in Aβ_{34-42} fibrils is not retained by the C-terminal residues in fibrils formed by full-length Aβ_{1-42}. In the final section of this paper, we summarize the

experimental EM, STEM, and solid-state NMR constraints on supramolecular structure by presenting a schematic structural model for Aβ_{10-35} and Aβ_{1-42} fibrils (also applicable to Aβ_{1-40} fibrils) that is consistent with these constraints.

MATERIALS AND METHODS

Peptide Synthesis and Fibrillization. Aβ peptides were synthesized on an Applied Biosystems model 433A automated synthesizer using standard fluorenylmethoxycarbonyl (FMOC) protocols with *H*-benzotriazol-1-yl-tetramethyluronium hexafluorophosphate activation. ^{13}C- and ^{15}N-labeled amino acids with FMOC protection were obtained from Cambridge Isotopes Laboratories and Isotec. Aβ_{1-42} was synthesized on preloaded Wang resins. Aβ_{10-35} and A$\beta_{10-35,Scr}$ were synthesized on Rink amide resins. Peptides were cleaved from the synthesis resins with a solution of phenol, ethanedithiol, and thioanisole in 95% trifluoroacetic acid (TFA) for approximately 90 min and then precipitated from the cleavage solution in cold *tert*-butyl methyl ether (TBME). Precipitated peptides were washed several times with cold TBME, dissolved in water, and lyophilized. Peptides were then purified by high-performance liquid chromatography (HPLC) at 55 °C, using a Vydac C18 column and a water/acetonitrile gradient with 0.1% TFA. The purity of Aβ_{1-42} determined by electrospray mass spectrometry was 93%. For Aβ_{10-35}, electrospray mass spectra showed a species with mass 17 units less than expected, comprising up to 15% of the purified product. This species was found to be entirely absent from mass spectra obtained with matrix-assisted laser desorption ionization, which indicate >95% purity. Final yields of purified peptides were roughly 50% of the theoretical maximum for Aβ_{10-35} and 15% for Aβ_{1-42}. After lyophilization of HPLC fractions containing purified peptide, peptides were fibrillized by dissolution in water at approximately 0.2 mM concentration for Aβ_{10-35} and 0.1 mM concentration for Aβ_{1-42}, with the pH adjusted as necessary by dropwise addition of dilute NaOH or acetic acid and with addition of 0.01% NaN_3. Peptide solutions were incubated at room temperature for 3−15 days with gentle rocking. Aliquots of incubated solutions were taken for EM measurements after 3−5 days. Amyloid fibril formation was verified by EM images of negatively stained samples and by solid-state NMR spectroscopy (see Results). Incubated solutions were lyophilized for solid-state NMR measurements. Solid-state NMR samples contained 3−10 mg of peptide. Measurements on unfibrillized peptides were performed directly on the lyophilized, HPLC-purified material, without incubation.

Electron Microscopy. For EM images, carbon film substrates were prepared by evaporation from a carbon rod source onto freshly cleaved mica in an Edwards Auto 306 coating system. Films were floated off in deionized water and picked up on lacy Formvar/carbon films (EM Sciences) supported on 200 mesh copper grids. Grids were glow-discharged in air prior to peptide deposition. Aliquots (5 μL) of incubated or fibrillized peptide solution were applied to EM grids and allowed to adsorb for 2 min. Grids were then washed 10 times by applying successive drops of deionized water and drawing off the excess liquid before negative staining by passing through two drops of 1% uranyl acetate. Excess fluid was blotted off and grids were allowed to dry in air. Transmission electron micrographs were recorded using a Philips/FEI CM120 electron microscope and Gatan GIF100 imaging filter equipped with a cooled slow-scan CCD camera. Images were acquired and processed by means of the Digital Micrograph program (Gatan).

MPL measurements were performed by scanning transmission electron microscopy (*46*). Aliquots of fibrillized peptide solutions were applied to grids covered by 3 nm carbon films and allowed to adsorb for 8 min. A mass calibration standard of tobacco mosaic virus (TMV) at a concentration of 0.4 μg/μL was injected into the solutions and allowed to adsorb for 2 min. Grids were then washed 10 times. After partial blotting to maintain a thin layer of water, the grids were immediately frozen by plunging into liquid ethane at −180 °C by means of a Leica KF80 freezing device. Specimens were transferred at −170 °C into a VG Microscopes HB501 field-emission STEM and were freeze-dried by warming slowly to −100 °C. After recooling the specimens, annular dark-field images containing 1024 × 1024 pixels were acquired at an accelerating voltage of 100 kV using a 1 nm probe diameter and a current of 2 pA to provide an electron dose of approximately 10^3 e/nm^2. Images were quantified using the NIH IMAGE program. MPL values were determined from the STEM images as described in the Results.

Solid-State NMR Spectroscopy. NMR measurements were performed on Varian/Chemagnetics Infinity-400 spectrometers, operating at ^{13}C NMR frequencies of 100.4 and 100.8 MHz. Varian/Chemagnetics magic-angle spinning (MAS) probes with 3.2 mm diameter rotors were used in all measurements. One-dimensional ^{13}C NMR spectra were obtained with cross-polarization and with proton decoupling at 100−120 kHz. ^{13}C chemical shifts are referenced to an external adamantane sample, with the chemical shift of the methylene ^{13}C NMR line taken to be 38.56 ppm relative to tetramethylsilane (TMS). MQ NMR data were obtained without MAS as previously described (*17*, *31*, *47*), using the MQ excitation pulse sequence of Suter et al. (*48*) to excite all MQ orders and starting with transverse ^{13}C magnetization. Radio frequency (rf) pulse lengths in the MQ excitation sequence were adjusted to maximize the amplitude of high-order MQ signals from a polycrystalline [$^{13}C_\epsilon$]-L-methionine setup sample immediately before MQ NMR data were acquired on Aβ samples. ^{13}C−^{13}C dipolar recoupling measurements were performed with the constant-time finite-pulse radio frequency-driven recoupling (fpRFDR-CT) technique of Ishii et al. (*49*), at a MAS frequency of 20.0 kHz and with π/2 and π pulse lengths of 5 and 15 μs, respectively. In the notation of Ishii et al. (*49*), fpRFDR-CT data were acquired with an initial *N* value of 64, decremented in units of 4, and with $K = 4$, leading to a total recoupling period of 76.8 ms and effective dipolar dephasing periods from 0 to 72 ms in increments of 4.8 ms. Proton decoupling fields during the recoupling period were 100−120 kHz. ^{13}C rf pulse amplitudes in the fpRFDR-CT sequence were optimized by maximizing the signal from a polycrystalline [1-^{13}C]-L-alanine setup sample at $N = 64$. ^{13}C-detected, ^{15}N−^{13}C rotational echo double resonance (REDOR) data were acquired with the pulse sequence of Anderson et al. (*50*, *51*) at a MAS frequency of 5.0 kHz. ^{13}C and ^{15}N π pulse lengths in the REDOR dephasing period were 10.0 μs. Pulse amplitudes were optimized by maximizing the REDOR dephasing effect on a polycrystalline [1-^{13}C,^{15}N]glycine setup

sample. Proton decoupling fields during the dephasing period were 100 kHz.

Possible artifacts due to spectrometer instabilities were minimized in all experiments by block averaging. Rf pulse sequences were actively synchronized with a MAS tachometer signal in fpRFDR-CT and REDOR experiments. Total signal acquisition times for each Aβ sample were approximately 100 h for MQ NMR data, 12−24 h for fpRFDR-CT data, and 12−36 h for REDOR data, with recycle delays of 1.5−4 s. The sensitivities of fpRFDR-CT and REDOR measurements, but not MQ NMR measurements, were enhanced by pulsed spin lock (PSL) detection (*52*).

Simulations of Solid-State NMR Data. MQ NMR data were simulated by numerical quantum mechanical calculations as previously described (*17*, *47*), representing the candidate β-sheet organizations by six ^{13}C spins (representing the ^{13}C labels) at positions indicated in Figure 6, with three additional spins placed at random positions in a rectangular box around the labels with a volume of 15 nm^3 to represent natural-abundance ^{13}C nuclei close to the labels. D_1 was set to 0.48 nm, the interchain spacing in both parallel and antiparallel β-sheets. D_2 was set to 1.02 nm, the estimated distance between labeled Ala21 sites in a hypothetical in-register antiparallel β-sheet structure. Additional displacements above and below the plane of the β-sheets were set to 0.15 nm for the methyl ^{13}C labels in simulations. MQ NMR simulations were averaged over 1024 orientations and random configurations of the three additional spins. Natural-abundance ^{13}C nuclei that are more distant from the ^{13}C labels also contribute to the experimental MQ NMR signals but cannot be included in the quantum mechanical simulations (which become prohibitively time-consuming for systems of more than nine spins). Experiments on unlabeled peptide samples indicate that natural-abundance ^{13}C nuclei only contribute significantly to one-quantum and two-quantum signals (because dipole-coupled groups of more than two natural-abundance ^{13}C nuclei are rare). To account for these contributions, quantities q_1 and q_2 were added to the simulated one-quantum and two-quantum signal amplitudes in Figure 8, with $q_1/q_2 = 25$, 13, and 9 for simulations at $\tau_{MQ} = 4.8$, 9.6, and 14.4 ms, respectively, and with $q_1 + q_2$ set to 24% of the sum of all MQ amplitudes resulting from the nine-spin numerical simulations. These values of q_1/q_2 represent typical ratios observed in MQ NMR measurements on unlabeled peptide samples, and the value of $q_1 + q_2$ was determined from the ratio of unlabeled aliphatic carbons to labeled sites in Aβ_{10-35}, assuming a 1.1% natural abundance of ^{13}C at the unlabeled sites. This approximate correction for MQ NMR signals from distant natural-abundance ^{13}C nuclei improves the agreement between experimental and simulated one-quantum amplitudes in Figure 8 but has no effect on the interpretation of the MQ NMR data in terms of the β-sheet organization in amyloid fibrils.

Simulations of fpRFDR-CT data in Figure 9c were also carried out by numerical quantum mechanical calculations, assuming six ^{13}C spins in a linear chain and averaging over 512 orientations. These simulations were performed at the average Hamiltonian level, assuming the average dipole−dipole Hamiltonian given by Ishii et al. (*49*). Average Hamiltonian calculations for fpRFDR-CT data include effects due to finite π pulses (which give rise to homonuclear dipolar recoupling in the limit of high-speed MAS) but treat the $\pi/2$ pulses in the fpRFDR-CT sequence as instantaneous rotations. Simulations of REDOR data in Figure 10a were also performed at the average Hamiltonian level, including a spin system of one ^{13}C nucleus and two ^{15}N nuclei with only heteronuclear dipole−dipole couplings. REDOR simulations were averaged over 4096 orientations.

Contributions of Background Signals to REDOR and fpRFDR-CT Data. ^{13}C NMR signals from natural-abundance ^{13}C nuclei and from residual unfibrillized peptide molecules contribute to both REDOR and fpRFDR-CT data. Because NMR signals in these measurements were detected under PSL (*52*), signals from the ^{13}C-labeled sites were not fully resolved from natural-abundance signals from unlabeled sites. Comparisons of NMR peak areas in ^{13}C MAS spectra of Aβ_{10-35} fibrils obtained with and without PSL indicate that all carbonyl (both labeled and unlabeled), all carboxyl, and all aromatic carbon sites (total of 55 sites) contribute to the REDOR data on Aβ_{10-35} fibrils in Figure 10a. All methyl (both labeled and unlabeled) sites and approximately nine other natural-abundance aliphatic carbon sites (total of 26 sites) contribute to the fpRFDR-CT data in Figure 9a.

The REDOR data plotted in Figure 10 can be expressed as

$$\Delta S/S_0 = \left(\frac{S_0^{\,l,f} + S_0^{\,na,d} - S_1^{\,l,f} - S_1^{\,na,d}}{S_0^{\,l,f} + S_0^{\,na,d}}\right)\left(\frac{S_0^{\,l,f} + S_0^{\,na,d}}{S_{tot}}\right) \quad (1a)$$

$$= (\Delta S/S_0)_i F \quad (1b)$$

$$S_{tot} = S_0^{\,l,f} + S_0^{\,l,u} + S_0^{\,na,d} + S_0^{\,na,u} \quad (2)$$

where $S_x^{\,l,f}$ is the ^{13}C NMR signal from labeled sites in fibrillized peptides, $S_x^{\,l,u}$ is the signal from labeled sites in unfibrillized peptides, $S_x^{\,na,d}$ is the signal from natural-abundance sites that are sufficiently close to ^{15}N-labeled sites to be dephased by ^{15}N−^{13}C couplings, and $S_x^{\,na,u}$ is the signal from natural-abundance sites that are more distant from ^{15}N labels. Subscripts $x = 1$ and $x = 0$ indicate signals with and without ^{15}N pulses. $(\Delta S/S_0)_i$ is the REDOR data that would be obtained in the absence of signal contributions from undephased natural-abundance ^{13}C and from undephased ^{13}C labels in unfibrillized peptides. F is the scaling factor that relates data for this ideal case to the actual experimental data. Given the 1.1% natural abundance of ^{13}C, given that Aβ_{10-35} contains 55 carbonyl, carboxyl, and aromatic sites, and given that 50% of the Aβ_{10-35} molecules in the REDOR measurements in Figure 10a contain a single ^{13}C label, we calculate $(S_0^{\,l,f} + S_0^{\,l,u})/S_{tot} = 0.46$ and $(S_0^{\,na,d} + S_0^{\,na,u})/S_{tot} = 0.54$. To determine the fraction of natural-abundance ^{13}C signal that is dephased under the experimental conditions in Figure 10a, separate REDOR measurements were performed on an Aβ_{10-35} fibril sample with a single ^{15}N label at F20 and no ^{13}C labels (data not shown). In these measurements, 18 ± 4% of the ^{13}C signal was dephased. Taking into account the 1:1 mixing of ^{15}N-labeled and ^{13}C-labeled peptides in Figure 10a, we estimate $S_0^{\,na,d} \approx 0.09(S_0^{\,na,d} + S_0^{\,na,u})$. Assuming that approximately 20% of the Aβ_{10-35} molecules are unfibrillized, so that $S_0^{\,l,f} \approx 0.80(S_0^{\,l,f} + S_0^{\,l,u})$, we then calculate $F \approx 0.41$. This estimate for F is in excellent agreement with the results in Figure 10a, in which a scaling factor of 0.43 is applied to simulations (which do not include signal contribu-

tions from unfibrillized peptides and from natural-abundance ^{13}C) in order to optimize the fit to experimental data.

Experimental data in fpRFDR-CT measurements can be expressed as the sum of four contributions as in eq 2, but with $S_0^{na,d}$ and $S_0^{na,u}$ referring to signals from natural-abundance ^{13}C nuclei that are in the proximity of or distant from other ^{13}C nuclei, respectively. The quantity $G \equiv (S_0^{l,u} + S_0^{na,u})/S_{tot}$ then represents the fraction of ^{13}C signal that does not decay to zero in experimental fpRFDR-CT data. For the data in Figure 9a, with the conditions stated above, $(S_0^{l,u} + S_0^{l,f})/S_{tot} \approx 0.78$ and $(S_0^{na,d} + S_0^{na,u})/S_{tot} \approx 0.22$. Again assuming that approximately 20% of peptide molecules are unfibrillized and that 90% of the natural-abundance signal does not dephase in fpRFDR-CT experiments, we calculate $G \approx 0.35$. This estimate is in good agreement with the experimental result that approximately 38% of the ^{13}C signal does not decay in Figure 9a.

Figure 9b reports the results of fpRFDR-CT experiments on Aβ_{1-42} fibrils with ^{13}C labels at both the Leu34 carbonyl and the Ala21 methyl carbon sites. In analogy to the case of Aβ_{10-35} described above, a total of approximately 41 carbon sites, with one ^{13}C label, contribute to the methyl fpRFDR-CT data. A total of 84 carbon sites, with one ^{13}C label, contribute to the carbonyl fpRFDR-CT data. For the methyl data, $(S_0^{l,u} + S_0^{l,f})/S_{tot} \approx 0.69$ and $(S_0^{na,d} + S_0^{na,u})/S_{tot} \approx 0.31$. For the carbonyl data, $(S_0^{l,u} + S_0^{l,f})/S_{tot} \approx 0.52$ and $(S_0^{na,d} + S_0^{na,u})/S_{tot} \approx 0.48$. Assuming that approximately 10% of Aβ_{1-42} molecules are unfibrillized and that 90% of the natural-abundance signal does not dephase in fpRFDR-CT experiments, $G \approx 0.35$ for the methyl data and $G \approx 0.48$ for the carbonyl data. These estimates are in good agreement with the experimental result that approximately 30% of the methyl signal and approximately 50% of the carbonyl ^{13}C signal do not decay in Figure 9b.

RESULTS

Electron Microscopy of Aβ_{10-35} Fibrils. Figure 2 shows EM images of negatively stained Aβ_{10-35} and A$\beta_{10-35,Scr}$ samples after incubation at pH 3.7 or 7.4. The pH value of 3.7 was chosen because this was the unadjusted pH after dissolution of lyophilized, purified Aβ_{10-35}. At pH 3.7 (Figure 2a,b), Aβ_{10-35} forms apparently single filaments with quite uniform morphology and with diameters of 6.6 ± 0.6 nm. At pH 7.4 (Figure 2c−f), Aβ_{10-35} fibrils display substantially more heterogeneous morphologies. These fibrils appear to be twisted pairs of single filaments with varying periodicities of twist. Fibril diameters vary from 5.5 ± 1.0 nm at the narrowest points to 10.5 ± 1.0 nm at the widest points. The fibrils at pH 7.4 have a tendency to aggregate laterally. The dependence of fibril morphology on pH seen in these EM images correlates with solid-state NMR and STEM data presented below. Dependence of fibril morphology on pH has been reported previously for Aβ_{10-35} (*16*). Twisted morphologies are commonly observed in EM and atomic force microscope (AFM) images of Aβ (*53*−*55*) and other amyloid fibrils.

Under similar incubation conditions at pH 7.4, A$\beta_{10-35,Scr}$ appears not to form well-ordered fibrils. Instead, nonfibrillar aggregates are observed in EM images of negatively stained samples (Figure 2g,h). The absence of visible amyloid fibrils of A$\beta_{10-35,Scr}$ is consistent with previous evidence that the central hydrophobic segment of Aβ_{10-35} plays an important role in the stabilization of the amyloid fibril structure (*38*, *45*). The EM results for A$\beta_{10-35,Scr}$ correlate with solid-state NMR data presented below.

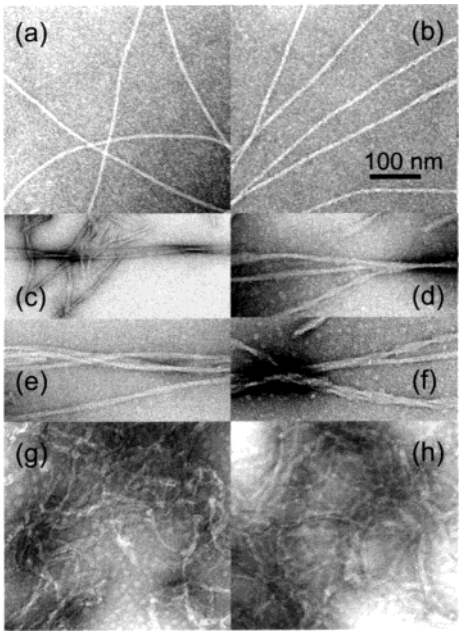

FIGURE 2: Electron micrographs of negatively stained Aβ_{10-35} fibrils prepared at pH 3.7 (a, b), Aβ_{10-35} fibrils prepared at pH 7.4 (c−f), and nonfibrillar A$\beta_{10-35,Scr}$ aggregates formed at pH 7.4 (g, h). Aβ_{10-35} fibril morphology depends strongly on pH. A$\beta_{10-35,Scr}$ does not fibrillize under the conditions of these experiments.

Figure 3 shows STEM images of unstained Aβ_{10-35} fibrils formed at pH 3.7 (Figure 3a) and pH 7.4 (Figure 3c). The intensity in these STEM images is directly proportional to mass density per unit area, after subtraction of background intensity due to scattering from the carbon film. Thus, the MPL of the fibrils can be determined from the difference between the total intensity in rectangular areas of fixed length centered on apparently straight segments of fibrils and the total intensity in identical areas of background displaced slightly from the fibrils, as indicated in Figure 3. The constant of proportionality between intensity and mass density is determined from similar measurements on codeposited TMV particles in the same field, which have a known MPL of 131 kDa/nm. Multiple STEM images of Aβ_{10-35} fibrils and multiple fibrils in each image were measured. The resulting data for fibrils formed at pH 3.7 are plotted as a histogram in Figure 3b, after binning in units of 1 kDa/nm. The histogram is well described by a single Gaussian peak centered at 12.8 kDa/nm, with a full width at half-maximum (fwhm) of 5.5 kDa/nm. This fwhm value is attributable to statistical Poisson noise in the STEM signal counts at each pixel and to random variations in the density of the carbon support film. MPL data for fibrils prepared at pH 7.4 are plotted as a histogram in Figure 3d, after binning in units of 2 kDa/nm. In this case, the histogram is not well described by a single Gaussian peak. Values ranging from 15 to 120 kDa/nm are observed, with the majority of counts occurring in peaks between 20 and 34 kDa/nm and between 46 and 60 kDa/nm.

A common feature of many (*15*, *27*−*30*, *56*, *57*), but not all (*26*, *53*, *58*), structural models for amyloid fibrils is lamination of the β-sheets. In a hypothetical cross-β structure with β-strands precisely perpendicular to the fibril axis and

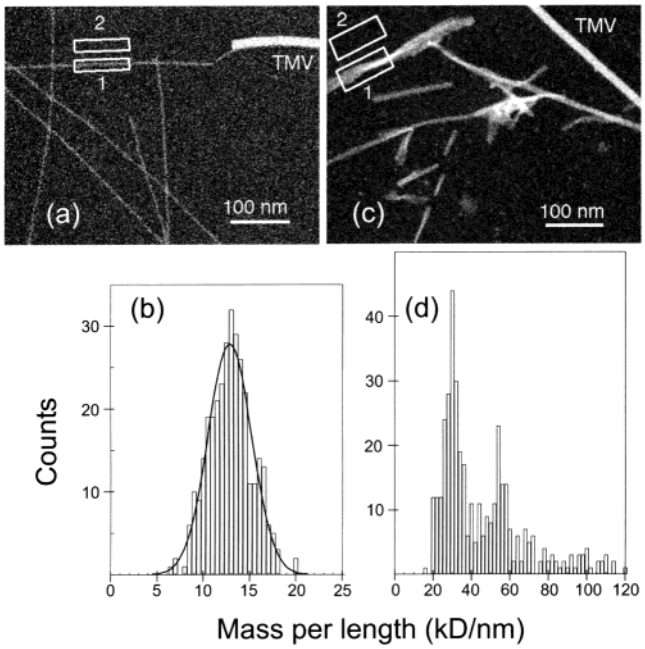

FIGURE 3: Scanning transmission electron micrographs of unstained Aβ_{10-35} fibrils prepared at pH 3.7 (a) and pH 7.4 (c). The mass per length (MPL) of amyloid fibrils is determined by integrating the image intensity in rectangular areas centered on the fibrils (rectangle 1 in panel a) and subtracting the intensity in identical areas of background (rectangle 2 in panel a). Intensities are calibrated by similar measurements on codeposited tobacco mosaic virus (TMV) particles. Histograms of MPL measurements on Aβ_{10-35} fibrils prepared at pH 3.7 (b) and pH 7.4 (d) indicate a strong pH dependence. A single cross-β sheet of Aβ_{10-35} with a 0.48 nm interchain spacing would have an MPL value of 6.0 kDa/nm.

with the entire peptide chain in a single extended β-strand, the MPL of a single lamina is simply the molecular mass divided by the 0.48 nm spacing between hydrogen-bonded peptide chains in a β-sheet. In the remainder of this paper, we use the term "cross-β unit" to describe any structural component with MPL equal to the MPL of this hypothetical cross-β lamina. By using this intentionally nonspecific term to discuss the STEM data, we mean to avoid unconfirmed assumptions about the folding of the β-sheets, the width of the β-sheets, or the presence of β-sheet lamination in the fibrils. Clearly, the MPL value alone does not uniquely determine any aspect of the fibril structure other than the number of peptide molecules per 0.48 nm displacement along the long axis of the fibril.

For Aβ_{10-35}, with molecular mass 2.902 kDa, the MPL of a single cross-β unit is 6.0 kDa/nm. The data in Figure 3b strongly suggest that Aβ_{10-35} fibrils formed at pH 3.7 are constructed exclusively from two cross-β units. We refer to this fibril structure, with MPL equal to that of two cross-β units, as the "protofilament" because this structure has the minimum MPL of all observed fibrils. The MPL histogram in Figure 3d suggests that the number of cross-β units in fibrils formed at pH 7.4 is not unique but ranges primarily between four and nine. The broad distribution of apparent MPL values in Figure 3d is at least partly a consequence of the tendency for the fibrils to associate laterally at pH 7.4 (see Figure 2c−f) and the difficulty of distinguishing single fibrils from laterally associated fibrils in the STEM images. Fibrils formed at pH 7.4 with MPL values of approximately 24 kDa/nm may be twisted pairs of the protofilaments observed at pH 3.7.

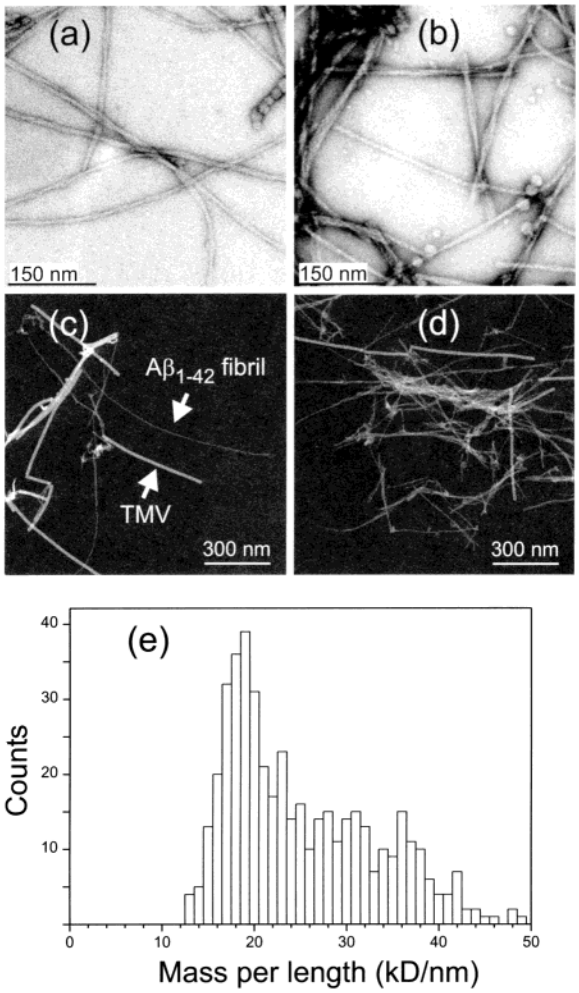

FIGURE 4: Negatively stained electron micrographs (a, b) and unstained scanning transmission electron micrographs (c, d) of Aβ_{1-42} fibrils prepared at pH 7.4 and a histogram of MPL values (e) determined as in Figure 3. A single cross-β sheet of Aβ_{1-42} with a 0.48 nm interchain spacing would have an MPL value of 9.4 kDa/nm.

Electron Microscopy of Aβ_{1-42} Fibrils. EM images of negatively stained Aβ_{1-42} fibrils formed at pH 7.4 are shown in Figure 4a,b. These fibrils exhibit obvious morphological heterogeneities, with variations in the periodicity of the apparent twist, the apparent diameter, and the degree of curvature. The majority of fibrils exhibit a periodic modulation of diameter, from minimum diameters of 6 ± 1 nm to maximum diameters of 12.5 ± 2.5 nm and with periods of 100 ± 40 nm. Apparently tightly twisted, drill-shaped fibrils with diameters of 6 ± 1 nm resemble fibrils identified at an early stage of incubation in earlier EM studies of Aβ_{1-40} fibrillization and classified as "type 1" by Goldsbury et al. (*54*). Apparently spherical aggregates of Aβ_{1-42}, with diameters of 10−20 nm, are also seen. Similar spherical structures have been observed previously in EM (*53*, *54*) and AFM (*59*) studies of Aβ fibrillization.

STEM images of unstained Aβ_{1-42} fibrils are shown in Figure 4c,d. Analysis of these images as described above results in the MPL histogram in Figure 4e. The histogram for Aβ_{1-42} shows a peak at 19 ± 2 kDa/nm and a tail at higher values, extending to 50 kDa/nm. Structures that are unambiguously single filaments (e.g., the Aβ_{1-42} fibril indicated in Figure 4c) have MPL values of approximately

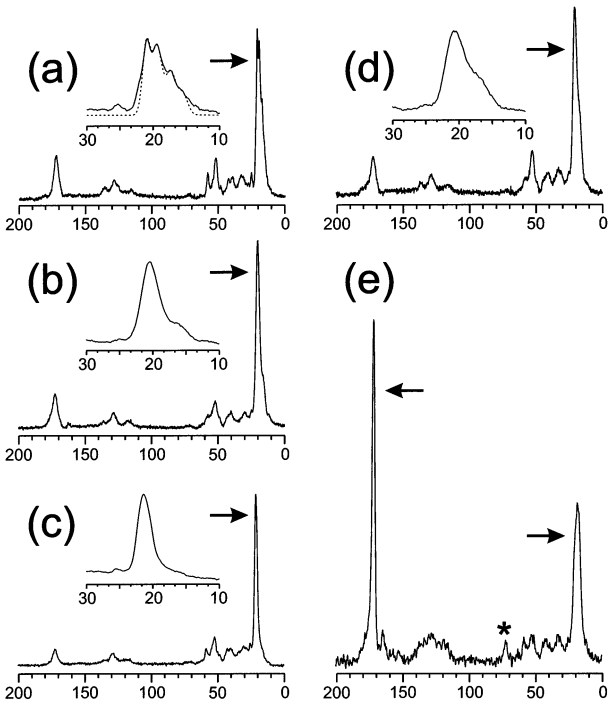

FIGURE 5: Solid-state ^{13}C MAS NMR spectra of Aβ_{10-35} fibrils prepared by incubation at pH 7.4 (a), unfibrillized Aβ_{10-35} (b), Aβ_{10-35} fibrils prepared by incubation at pH 3.7 (c), A$\beta_{10-35,Scr}$ incubated at pH 7.4 (d), and Aβ_{1-42} fibrils prepared by incubation at pH 7.4 (e). All samples are in lyophilized form. Arrows indicate signals from ^{13}C labels at the methyl carbon of Ala21 (a−e) and the carbonyl carbon of Leu34 (e). The asterisk in spectrum e indicates an MAS sideband line from the carbonyl label. Expansions of the methyl signal region are shown for spectra a−d. The dashed line in spectrum a is a fit of the methyl line shape to a sum of four Gaussian lines, centered at 21.1, 19.4, 17.4, and 15.6 ppm with widths of 1.4, 1.7, 1.8, and 1.8 ppm.

19 kDa/nm. Structures with higher MPL values are likely to be bundles of single fibrils. Given the molecular mass of 4.514 kDa for Aβ_{1-42}, the MPL of a single cross-β unit is 9.4 kDa/nm. The peak in the MPL histogram therefore appears to correspond to an Aβ_{1-42} protofilament constructed from two cross-β units. Higher MPL values observed in the STEM image analysis are attributed to bundled or overlapping fibrils that are difficult to distinguish from single protofilaments due to the relatively low resolution of the STEM images. The apparent number of laminae for all measured fibrils lies primarily in the range from two to four, suggesting that some fibrils may be pairs of protofilaments. Thus, unpaired Aβ_{1-42} protofilaments appear to coexist with paired protofilaments at pH 7.4, unlike the case of Aβ_{10-35} where only unpaired protofilaments are observed at pH 3.7 but no unpaired protofilaments are observed at pH 7.4.

One-Dimensional Solid-State ^{13}C NMR Spectroscopy of Amyloid Fibrils. Figure 5 shows 1D solid-state ^{13}C NMR spectra of Aβ peptides, obtained with standard MAS, cross-polarization, and high-power proton decoupling techniques to provide adequate sensitivity and high spectral resolution. Panels a and b of Figure 5 are spectra of Aβ_{10-35}, ^{13}C-labeled at the methyl carbon of Ala21, after fibrillization at pH 7.4 and before fibrillization (but after purification and lyophilization), respectively. Fibrillization induces characteristic changes in the ^{13}C NMR signals. Most strikingly, the natural-abundance aliphatic signals between 25 and 60 ppm develop sharper features, including a well-resolved peak at 58 ppm attributable to a subset of the α-carbons in the peptide backbone. In addition, the width (fwhm) of the natural-abundance carbonyl peak at 172 ppm is reduced from 6 to 4 ppm. These changes in natural-abundance ^{13}C NMR signals serve as an empirical indication that the majority of Aβ_{10-35} molecules in the sample are in fibrils, rather than in nonfibrillar aggregates. Similar features are observed in solid-state ^{13}C NMR spectra of Aβ_{1-40} fibrils (*17*, *20*).

Upon fibrillization of Aβ_{10-35} at pH 7.4, the strong signal at 20.3 ppm arising from the labeled Ala21 methyl carbon changes from a single peak with a width of 3.2 ppm to a series of partially resolved peaks at 21.0, 19.4, and 17.4 ppm with widths of approximately 1.4, 1.7, and 1.8 ppm and areas in an approximate 3:3:2 ratio. In contrast, as shown in Figure 5c, fibrillization of the same peptide at pH 3.7 produces a single ^{13}C NMR line for the Ala21 methyl carbon at 21.3 ppm with a width of 2.5 ppm. Incubation of A$\beta_{10-35,Scr}$ at pH 7.4 leads to a ^{13}C NMR spectrum that strongly resembles the spectrum of unfibrillized Aβ_{10-35}, as shown in Figure 5d.

The differences in Ala21 methyl ^{13}C NMR signals of Aβ_{10-35} fibrils prepared at pH 3.7 and 7.4 correlate with the differences in the corresponding EM images (Figures 2 and 3). Observation of a single ^{13}C NMR line suggests a single structural environment for Ala21 in the pH 3.7 fibrils, consistent with the homogeneous morphology in the EM images and the observation of a single peak in the MPL histogram. Observation of several partially resolved lines suggests several distinct structural environments for Ala21 in the pH 7.4 fibrils, consistent with the more heterogeneous and complex morphology in the EM images and the broad distribution of MPL values. The similarity between ^{13}C NMR spectra of incubated A$\beta_{10-35,Scr}$ and unfibrillized Aβ_{10-35} is consistent with the lack of visible amyloid fibrils in EM images of A$\beta_{10-35,Scr}$.

Figure 5e shows the 1D ^{13}C MAS NMR spectrum of Aβ_{1-42} after fibrillization at pH 7.4, with ^{13}C labels at the methyl carbon of Ala21 and the carbonyl carbon of Leu34 and with a ^{15}N label at the amide nitrogen of Val40. The signal from natural-abundance α-carbons (48−60 ppm) resembles that of well-fibrillized Aβ_{10-35}. The carbonyl ^{13}C label exhibits a single peak at 172.2 ppm with a width of 2.5 ppm. This relatively narrow carbonyl line indicates a high degree of structural order at Leu34. The methyl ^{13}C label exhibits a single peak at 19.0 ppm with a width of 5.5 ppm. The morphological heterogeneity seen in the EM images of this Aβ_{1-42} sample may be associated with a larger degree of structural heterogeneity at Ala21 than at Leu34.

Multiple-Quantum ^{13}C NMR Measurements on Aβ_{10-35} Fibrils. As previously demonstrated for Aβ_{1-40} and Aβ_{16-22} fibrils (*17*, *18*), ^{13}C MQ NMR spectroscopy (*31*, *47*) can be used to probe the supramolecular organization of β-sheets in amyloid fibrils. As depicted in Figure 6a, if a single ^{13}C-labeled site is contained in a β-strand segment that forms a fully parallel and in-register β-sheet in the fibrils, the ^{13}C labels in a single β-sheet lamina form a nearly linear chain with internuclear spacings of approximately 0.48 nm. If the labeled site is contained in an antiparallel β-sheet in the fibrils, as in Figure 6b, the labels form a zigzag pattern with internuclear distances that exceed 0.48 nm and depend on the position of the labeled site within the β-strand segment. In a hypothetical dimeric or trimeric parallel β-sheet, as in

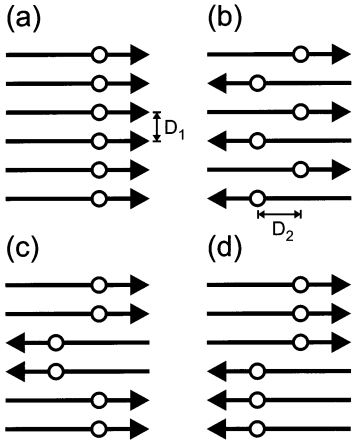

FIGURE 6: Candidate β-sheet organizations in amyloid fibrils considered in the analysis of multiple-quantum (MQ) NMR data: fully parallel (a), antiparallel (b), dimeric (c), and trimeric (d). Arrows represent peptide chains, with arrowheads at the C-termini. Open circles represent ^{13}C labels introduced at a single carbon site in each chain. The interchain spacing D_1 is approximately 0.48 nm in all β-sheets. The distance D_2 depends on the position of the label in the peptide chain in antiparallel structures.

Figure 6c,d, the ^{13}C labels occur as pairs or triplets with a 0.48 nm internuclear distance and with greater distances between pairs or triplets.

The structures in Figure 6 can be distinguished experimentally by solid-state NMR measurements that probe the strengths of nuclear magnetic dipole−dipole couplings among the ^{13}C labels, as represented by the dipole−dipole coupling constants $d = \gamma^2\hbar/2\pi R^3$, where R is the internuclear distance, γ is the nuclear magnetogyric ratio, and $\hbar$ is Planck's constant. At $R = 0.48$ nm, $d = 69$ Hz. In a MQ NMR measurement, NMR transitions in which groups of n nuclear spins flip simultaneously in the magnetic field of the spectrometer are excited and detected, using a MQ excitation sequence of length τ_{MQ}. For an n-quantum signal to be observable, at least n nuclear spins must be linked by dipole−dipole couplings of strength $d \sim \tau_{MQ}^{-1}$; i.e., they must be sufficiently close in space. Thus, for $\tau_{MQ} \sim 14$ ms, at a qualitative level one expects to detect only one-quantum signals in an antiparallel β-sheet, two-quantum signals in a dimeric parallel β-sheet, three-quantum signals in a trimeric parallel β-sheet, and n-quantum signals with $n > 3$ in a fully parallel β-sheet.

Figure 7 shows experimental MQ NMR spectra of fibrillized Aβ_{10-35} (Figure 7a,b for pH 7.4 and 3.7, respectively), incubated A$\beta_{10-35,Scr}$ (Figure 7c), and unfibrillized Aβ_{10-35} (Figure 7d). In all cases, the peptides are ^{13}C-labeled at the methyl carbon of Ala21 (same samples as in Figure 5a−d), and data are shown for $\tau_{MQ} = 4.8$, 9.6, and 14.4 ms. For Aβ_{10-35} fibrillized at either pH value, MQ NMR signals up to and including four quantum are observed above the noise level at $\tau_{MQ} = 14.4$ ms. According to the qualitative expectations outlined above, these MQ NMR data suggest a parallel organization of β-sheets in Aβ_{10-35} fibrils. Additionally, the similarity of MQ NMR signal amplitudes in Figure 8 indicates that the organization of β-sheets is not dependent on pH, despite the differences in fibril morphology, MPL, and 1D ^{13}C NMR spectra reported above. In contrast, only very weak three-quantum signals and no detectable four-quantum signals are observed in MQ NMR spectra of unfibrillized Aβ_{10-35} and incubated A$\beta_{10-35,Scr}$. At all values

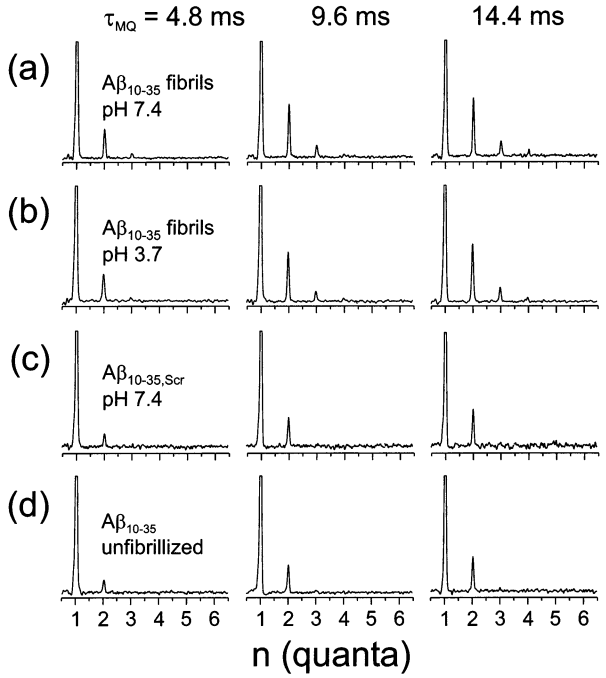

FIGURE 7: ^{13}C MQ NMR spectra of the indicated samples with ^{13}C labels at the methyl carbon of Ala21 for MQ excitation times $\tau_{MQ} = 4.8$, 9.6, and 14.4 ms. Each MQ NMR spectrum is a concatenation of subspectra for individual MQ orders from $n = 1$ to $n = 6$, with a 40 kHz spectral width in each subspectrum. Vertical scales are adjusted so that the peak in the one-quantum spectrum is clipped at 50% of its maximum value. In fibrillized samples, significant three- and four-quantum signals are detected, with amplitudes that increase relative to the one- and two-quantum signals as τ_{MQ} increases. In incubated (but not fibrillized, as in Figure 2g,h) A$\beta_{10-35,Scr}$ and unfibrillized Aβ_{10-35}, four-quantum signals are absent and three-quantum signals are absent or extremely weak at all values of τ_{MQ}.

of τ_{MQ}, two-quantum signals in MQ NMR spectra of unfibrillized Aβ_{10-35} and incubated A$\beta_{10-35,Scr}$ are significantly weaker relative to the one-quantum signals than in MQ NMR spectra of fibrillized Aβ_{10-35}. Two-quantum signals in Figure 7c,d are attributable to dipole−dipole couplings between ^{13}C labels and natural-abundance ^{13}C nuclei.

Quantitative analyses of MQ NMR data for Aβ_{10-35} fibrils are accomplished by comparison with numerical simulations. Figure 8 compares experimental MQ signal amplitudes with simulations for the four β-sheet organizations depicted in Figure 6. Experimental one-quantum amplitudes contain significant contributions from natural-abundance ^{13}C nuclei that can only be included in simulations at an approximate level (see Materials and Methods). Therefore, all experimental and simulated MQ amplitudes in Figure 8 are normalized to the two-quantum amplitude, and structural information is contained in the higher quantum amplitudes. Signal normalization is required because the overall experimental signal amplitudes decrease with increasing τ_{MQ}, due to spin relaxation processes, and because we have no absolute calibration of NMR signal amplitudes. For Aβ_{10-35} fibrils prepared at pH 7.4, the best agreement between experimental and simulated two-, three-, and four-quantum amplitudes at all values of τ_{MQ} is found for the fully parallel β-sheet simulations, although reasonable agreement is also found for the trimeric parallel β-sheet simulations. For Aβ_{10-35} fibrils prepared at pH 3.7, the fully parallel and trimeric β-sheet

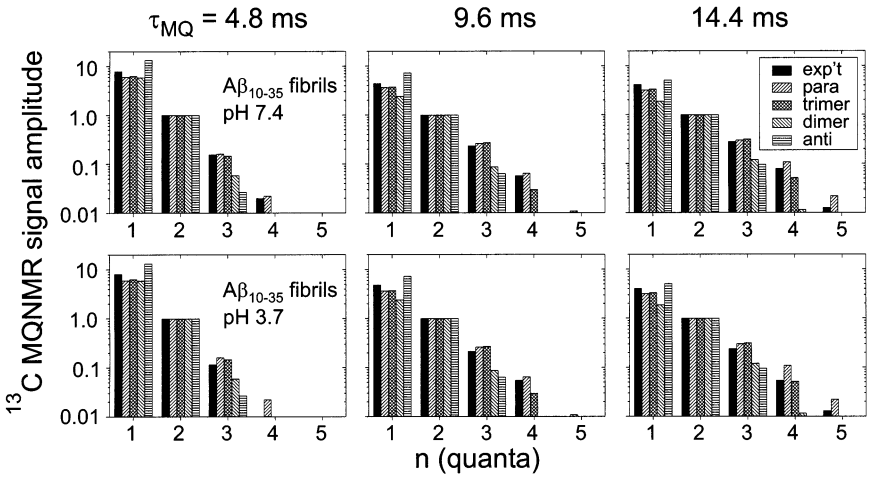

FIGURE 8: Comparison of experimental MQ NMR amplitudes for Aβ_{10-35} fibrils, obtained from peak areas in Figure 7, with simulated amplitudes for the four candidate β-sheet organizations in Figure 6. Experimental and simulated MQ amplitudes are normalized to the two-quantum amplitudes. Amplitudes are plotted on a logarithmic scale to permit assessment of three- and four-quantum amplitudes. Uncertainties in all experimental measurements due to noise in the MQ NMR spectra are approximately ± 0.06 ($2\sigma_{rms}$).

simulations give comparable agreement with experimental MQ amplitudes. The fully antiparallel and the dimeric β-sheet simulations yield substantially lower three- and four-quantum amplitudes and are clearly excluded by the experimental MQ data at both pH values. Thus, at a quantitative level, the MQ NMR data support a parallel organization of β-sheets in Aβ_{10-35} fibrils at both pH values, extending over at least three successive peptide chains.

The parallel β-sheet simulations in Figure 8 assume in-register alignment of Aβ_{10-35} chains, meaning that residue k of one chain is hydrogen bonded to residues k $-$ 1 and k $+$ 1 of a neighboring chain. Additional simulations were performed for a putative out-of-register parallel β-sheet structure in which the hydrogen-bonding pattern is shifted by one residue, so that residue k of one peptide chain is hydrogen bonded to either residues k $-$ 2 and k or residues k and k $+$ 2 of a neighboring chain. On the basis of molecular modeling of β-sheets, nearest-neighbor distances between methyl ^{13}C labels in the shifted structure were taken to alternate between 0.70 and 0.77 nm. Simulations for the shifted parallel β-sheet structure (not shown) yielded weaker three- and four-quantum signals, relative to the two-quantum signals, than simulations for either the in-register parallel β-sheet structure or the trimeric β-sheet structure. Comparison with the experimental data excludes out-of-register parallel β-sheet structures for Aβ_{10-35} fibrils at both pH values.

The antiparallel β-sheet simulations in Figure 8 also assume an in-register alignment, meaning that residue 10 $+$ k of one chain is hydrogen bonded to residue 35 $-$ k of a neighboring chain. A shifted antiparallel structure in which residue 10 $+$ k is hydrogen bonded to residue 32 $-$ k would be consistent with the MQ NMR data on Ala21-labeled Aβ_{10-35} fibrils but is ruled out by the additional solid-state NMR data described below.

^{13}C$-^{13}$C Dipolar Recoupling Measurements on Aβ_{10-35} and Aβ_{1-42} Fibrils. Additional solid-state NMR measurements were performed to test the β-sheet structure in the C-terminal hydrophobic segment of Aβ_{10-35} and in both hydrophobic segments of Aβ_{1-42}. These measurements employed the fpRFDR-CT technique developed by Ishii et al. (*49*). In fpRFDR-CT measurements on ^{13}C-labeled samples, the ^{13}C NMR signal intensity under high-speed MAS conditions is measured as a function of the effective dipolar dephasing time τ_D during which homonuclear dipole$-$dipole couplings are switched on by a recoupling pulse sequence. The rate of decay of the NMR signals with increasing τ_D serves as a measure of the strength of dipole$-$dipole couplings and hence ^{13}C$-^{13}$C distances. We have recently used fpRFDR-CT measurements to demonstrate an in-register parallel β-sheet organization in Aβ_{1-40} fibrils, with parallel alignment from Gly9 through Val39 (*20*).

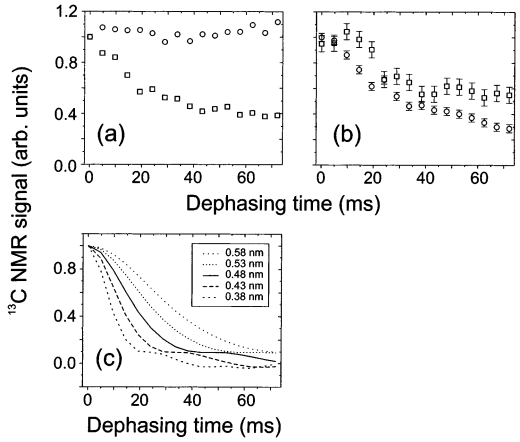

FIGURE 9: (a) Experimental ^{13}C$-^{13}$C dipolar recoupling data for unfibrillized Aβ_{10-35} (circles) and Aβ_{10-35} fibrils prepared at pH 7.4 (squares), obtained with the fpRFDR-CT solid-state NMR technique. Uncertainty due to noise in the experimental spectra is about equal to the size of the symbols. Both samples were synthesized with ^{13}C labels at the methyl carbons of Ala30. Decay of the methyl ^{13}C NMR signal with increasing dipolar dephasing time in the fibrillized sample indicates the presence of intermolecular ^{13}C$-^{13}$C dipole$-$dipole couplings. (b) Dipolar recoupling data for Aβ_{1-42} fibrils prepared at pH 7.4. Squares represent data for a ^{13}C label at the carbonyl carbon of Leu34. Circles represent data for a ^{13}C label at the methyl carbon of Ala21. Error bars indicate the root-mean-squared noise (σ_{rms}) in the experimental spectra. (c) Simulated dipolar recoupling curves for linear chains of ^{13}C nuclei with the indicated internuclear distances.

Figure 9a shows experimental fpRFDR-CT data for fibrillized and unfibrillized samples of Aβ_{10-35}, ^{13}C-labeled at the methyl carbon of Ala30. ^{13}C NMR signals of the unfibrillized sample do not decay measurably up to 72 ms,

the maximum value of τ_D in these experiments, indicating the absence of measurable $^{13}C-^{13}C$ couplings. The fibrillized sample exhibits a significant signal decay on the time scale of 40 ms. Figure 9b shows experimental data for fibrillized Aβ_{1-42}, ^{13}C-labeled at the methyl carbon of Ala21 and the carbonyl carbon of Leu34 and ^{15}N-labeled at Val40 (same sample as in Figure 5e). ^{13}C NMR signals from both labeled sites, measured in separate fpRFDR-CT experiments in which the ^{13}C rf carrier frequency was set to either the methyl or the carbonyl NMR frequency, decay significantly on the time scale of 40 ms. Figure 9c shows simulated fpRFDR-CT decay curves for linear chains of ^{13}C nuclei with internuclear spacings ranging from 0.38 to 0.58 nm. The time scale for decay of ^{13}C NMR signals in the experimental data for fibrillized Aβ_{10-35} and Aβ_{1-42} matches the time scale in simulations for internuclear spacings of approximately 0.48 $\pm$ 0.05 nm, consistent with in-register parallel β-sheet structures for both peptides at the labeled sites.

In experimental fpRFDR-CT data (Figure 9a,b), the NMR signals decay to 30−50% of their initial amplitudes. In simulations (Figure 10c), the signals decay nearly to zero. As demonstrated quantitatively in Materials and Methods, this difference between experiments and simulations is due to experimental signal contributions from natural-abundance ^{13}C nuclei and from ^{13}C labels in residual unfibrillized peptides, which would decay only at larger values of τ_D.

$^{15}N-^{13}C$ REDOR Measurements on Aβ_{10-35} and Aβ_{1-42} Fibrils. Figure 10a shows data obtained with the REDOR technique (*50*, *51*) for fibrils prepared at pH 7.4 from an equimolar mixture of Aβ_{10-35} molecules labeled with ^{13}C at the carbonyl site of Phe19 or with ^{15}N at Phe20. In a ^{13}C-detected, $^{15}N-^{13}C$ REDOR experiment, one measures the amplitude of the ^{13}C MAS NMR signal as a function of a heteronuclear dipolar dephasing time τ_{RED} during which a rotor-synchronized rf pulse train is applied to ^{13}C nuclei only (S_0 signal) or to both ^{13}C and ^{15}N nuclei (S_1 signal). As usual, the REDOR data are plotted as $\Delta S/S_0 \equiv (S_0 - S_1)/S_0$ to cancel out dependences on τ_{RED} due to effects other than $^{13}C-^{15}N$ couplings. In Figure 10a, a significant buildup of $\Delta S/S_0$ is observed on a time scale of 30 ms. As shown in Figure 10b, in an in-register parallel β-sheet structure, the carbonyl group of Phe19 is hydrogen bonded to the amide group of Phe20, leading to distances $r_1 \approx 0.41$ nm and $r_2 \approx 0.56$ nm between the ^{13}C label and ^{15}N labels on neighboring peptide chains, with an angle of approximately 150° between r_1 and r_2. Because the REDOR sample was fibrillized from a 1:1 mixture of ^{13}C-labeled and ^{15}N-labeled Aβ_{10-35} molecules, we expect 25% of the ^{13}C labels to be coupled to one ^{15}N label at r_1, 25% of the ^{13}C labels to be coupled to one ^{15}N label at r_2, 25% of the ^{13}C labels to be coupled to ^{15}N labels at both r_1 and r_2, and 25% of the ^{13}C labels to have no nearby ^{15}N labels. The simulated REDOR curve in Figure 10a, calculated as the sum of curves for these four cases, shows a buildup of $\Delta S/S_0$ on the same time scale as the experimental data for Aβ_{10-35} fibrils.

The simulated REDOR curve in Figure 10a was scaled by a factor of 0.43 to optimize the fit to the experimental values. This scaling factor accounts for contributions to the experimental REDOR data from natural-abundance ^{13}C background signals and from an estimated 20% of the Aβ_{10-35} molecules that are in nonfibrillar aggregates and therefore do not participate in the parallel β-sheet structure

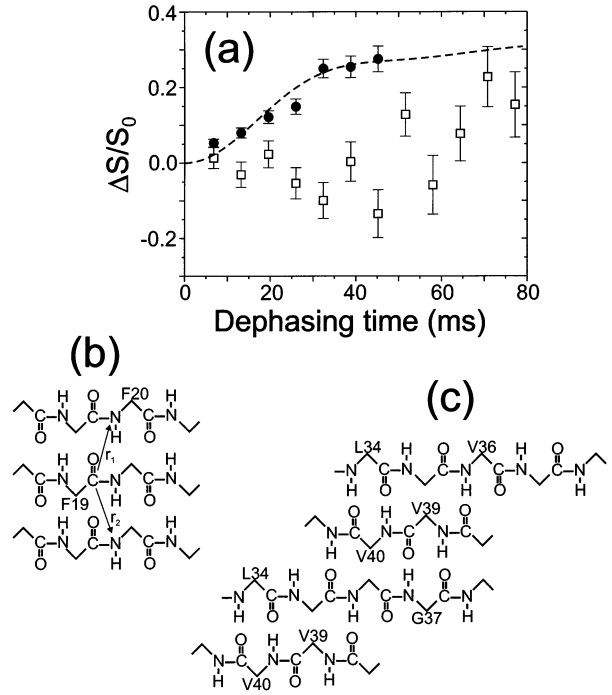

FIGURE 10: (a) Experimental $^{15}N-^{13}C$ dipolar recoupling data for Aβ_{10-35} fibrils prepared at pH 7.4 (filled circles) and Aβ_{1-42} fibrils prepared at pH 7.4 (open squares), obtained with the REDOR solid-state NMR technique. Error bars indicate uncertainty due to the root-mean-squared noise (σ_{rms}) in the experimental spectra. The Aβ_{10-35} fibrils were prepared from an equimolar mixture of peptides labeled with either ^{13}C at the carbonyl carbon of Phe19 or ^{15}N at the amide nitrogen of Phe20. The Aβ_{1-42} fibrils were prepared with ^{13}C labels at the methyl carbon of Ala21 and the carbonyl carbon of Leu34 and with ^{15}N labels at the amide nitrogen of Val40. (b) Portion of an in-register parallel β-sheet structure for Aβ_{10-35} fibrils showing the inequivalent distances r_1 and r_2 between the carbonyl carbon of Phe19 and the amide nitrogen of Phe20. REDOR simulations (dashed line in part a) assume $r_1 = 0.414$ nm, $r_2 = 0.560$ nm, and an angle of 154° between r_1 and r_2. (c) Portion of the antiparallel β-sheet structure determined for Aβ_{34-42} fibrils by Lansbury, Griffin, and co-workers (*11*), in which each Leu34 carbonyl carbon is approximately 0.41 nm from a hydrogen-bonded Val40 amide nitrogen. The REDOR data (open squares in part a) indicate that this antiparallel β-sheet structure is not present in Aβ_{1-42} fibrils.

(see Materials and Methods for quantitative treatment of these contributions). In these simulations, it is sufficient to consider only the two nearest-neighbor ^{15}N sites, as depicted in Figure 10b, because other ^{15}N sites would be at least 0.8 nm from the ^{13}C-labeled carbonyl site and therefore would not have significant $^{15}N-^{13}C$ dipole−dipole couplings (less than 5 Hz).

Figure 10a also shows experimental REDOR data for Aβ_{1-42} fibrils (same sample as Figures 5e and 9b). These data test for possible intermolecular dipole−dipole coupling between the ^{13}C label at the carbonyl site of Leu34 and the ^{15}N label at Val40 in this Aβ_{1-42} sample. A measurable $^{13}C-^{15}N$ coupling is not expected in the in-register parallel β-sheet structure supported by the fpRFDR-CT data on Aβ_{1-42} fibrils (Figure 9b), where $^{13}C-^{15}N$ distances within one β-sheet would exceed 1.5 nm and $^{13}C-^{15}N$ dipole−dipole couplings would therefore be less than 1 Hz. In contrast, $^{13}C-^{15}N$ couplings comparable in strength to those detected in the REDOR measurements on Aβ_{10-35} described above would be expected if the C-terminal hydrophobic segment of full-length Aβ_{1-42} adopted the same antiparallel structure as in

Table 1: ^{13}C NMR Chemical Shifts at Labeled Sites in Aβ Fibrils

fibril sample	^{13}C-labeled site	δ_{obs} (ppm)[a]	δ_{coil} (ppm)[b]
Aβ_{10-35}, pH 7.4	Ala21 methyl	21.0, 19.4, 17.4	17.4
Aβ_{10-35}, pH 7.4	Phe19 carbonyl	171.6	174.1
Aβ_{10-35}, pH 7.4	Ala30 methyl	19.7	17.4
Aβ_{10-35}, pH 3.7	Ala21 methyl	21.3	17.4
Aβ_{1-42}, pH 7.4	Ala21 methyl	19.0	17.4
Aβ_{1-42}, pH 7.4	Leu34 carbonyl	172.2	175.9

[a] Experimentally observed chemical shift relative to TMS in 1D MAS NMR spectra, based on external polycrystalline adamantane reference at 38.56 ppm. Uncertainty approximately 0.2 ppm. [b] Random coil chemical shift, taken from Wishart et al. (76) and adjusted to TMS reference by subtraction of 1.7 ppm.

fibrils formed by the Aβ_{34-42} fragment investigated by Lansbury, Griffin, and co-workers (*11*). The antiparallel β-sheet structure determined for Aβ_{34-42} fibrils is depicted in Figure 10c. In this structure, Leu34 of each Aβ_{34-42} chain is hydrogen bonded to Val40 of a neighboring chain, leading to ^{13}C$-^{15}$N distances of approximately 0.41 nm and coupling strengths of approximately 44 Hz. The experimental REDOR data (Figure 10a) indicate that ^{13}C$-^{15}$N couplings are much weaker than predicted for the antiparallel structure. The data indicate $\Delta S/S_0 < 0.05$ at $\tau_{RED} = 40$ ms, which implies that fewer than 15% of the fibrillized Aβ_{1-42} molecules participate in the antiparallel β-sheet structure (based on REDOR simulations for the antiparallel structure and taking into account signal contributions from natural-abundance ^{13}C and unfibrillized peptides as described above).

DISCUSSION

Interpretation of Structural Constraints from Solid-State NMR. In loose analogy to the usual description of globular protein structures, the levels of structure in an amyloid fibril may be termed primary, secondary, tertiary, and quaternary, with primary structure referring to the amino acid sequence, secondary structure referring to the conformation of individual peptide molecules, tertiary structure referring to the supramolecular organization of peptide molecules within one cross-β unit (as defined above), and quaternary structure referring to the organization of cross-β units within a fibril. With these definitions, the EM data presented above primarily place constraints on quaternary structure, while the solid-state NMR data place constraints on secondary and tertiary structure.

Constraints on secondary structure come from the ^{13}C NMR chemical shifts at isotopically labeled carbonyl and β-carbon sites in one-dimensional MAS NMR spectra (Figure 5). The empirical correlation of ^{13}C NMR chemical shifts with protein secondary structure has been established from both solid-state NMR (*18*, *22*, *60*, *61*) and liquid-state (*62*−*64*) NMR data. Observed chemical shifts from fibrillized Aβ samples δ_{obs} and random coil chemical shifts δ_{coil} are summarized in Table 1. The secondary shifts $\Delta\delta \equiv \delta_{obs} - \delta_{coil}$ are systematically positive for alanine methyl carbons and negative for carbonyl carbons. These secondary shifts are consistent with β-strand peptide backbone conformations at all labeled sites in both hydrophobic segments of Aβ_{10-35} and Aβ_{1-42} fibrils.

Constraints on tertiary structure come from ^{13}C MQ NMR, fpRFDR-CT, and REDOR data. The observation of significant three- and four-quantum NMR signals in MQ NMR spectra of Aβ_{10-35} fibrils prepared at either pH 7.4 or pH 3.7 (Figure 7) and the quantitative comparison of the experimental MQ signal amplitudes with simulations (Figure 8) indicate that ^{13}C labels introduced at the methyl carbon of Ala21, at the C-terminal end of the central hydrophobic segment, occur in groups of three or more with internuclear spacings less than approximately 0.55 nm. This result is consistent with an in-register parallel β-sheet organization of the central hydrophobic segment but is inconsistent with in-register antiparallel, dimeric parallel, or out-of-register parallel β-sheet organizations.

It is especially interesting that the experimental MQ NMR data for Aβ_{10-35} fibrils are nearly identical at pH 7.4 and 3.7, despite the qualitative differences in the 1D ^{13}C NMR spectra (Figure 5a,c) and the EM data (Figures 2 and 3). Electrostatic interactions are expected to be different at pH 3.7 and 7.4 due to pH-dependent side chain charges (see below). Differences in quaternary structure, but not tertiary structure, may then be due to electrostatic interactions.

The fpRFDR-CT data indicate distances of 0.48 ± 0.05 nm between ^{13}C labels at Ala30 methyl carbons in Aβ_{10-35} fibrils (Figure 9a) and between ^{13}C labels at both Ala21 methyl carbons and Leu34 carbonyl carbons in Aβ_{1-42} fibrils (Figure 9b). REDOR data on Aβ_{10-35} fibrils (Figure 10a) are consistent with hydrogen bonding between the carbonyl group of Phe19 and the amide group of Phe20. Thus, at least four distinct solid-state NMR techniques, i.e., DRAWS (dipolar recoupling with a windowless sequence) (*13*, *14*, *16*, *65*), MQ NMR, fpRFDR-CT, and REDOR, applied to samples with labels at multiple distinct sites all support the same in-register parallel β-sheet organization in Aβ_{10-35} fibrils, making it rather unlikely that an unforeseen experimental artifact could explain the solid-state NMR results. REDOR measurements on Aβ_{1-42} fibrils, designed to test for an antiparallel β-sheet organization in the C-terminal hydrophobic segment analogous to the antiparallel organization reported for Aβ_{34-42} fibrils (*11*), give a negative result (Figure 10a) and are also consistent with a parallel β-sheet organization.

The chemical shift, fpRFDR-CT, and REDOR data on Aβ_{1-42} fibrils reported above represent the first secondary and tertiary structural constraints on Aβ_{1-42} fibrils from solid-state NMR. These constraints, which are consistent with solid-state NMR data on Aβ_{1-40} fibrils (*17*, *20*), support the view that the structure of Aβ_{1-42} fibrils is not significantly different from that of Aβ_{1-40} fibrils, apart from the addition of two hydrophobic residues at the C-terminus. We find no evidence that the association of elevated Aβ_{1-42} levels with Alzheimer's disease (*34*) and the higher amyloidogenicity (*35*) of Aβ_{1-42} is attributable to differences in the supramolecular structure of Aβ_{1-40} and Aβ_{1-42} fibrils.

Perutz et al. have recently proposed a schematic model for the supramolecular organization of β-sheets in Aβ_{1-42} fibrils that includes both parallel and antiparallel alignments of neighboring peptide chains. This model is inconsistent with the observation of intermolecular distances of approximately 0.48 nm between ^{13}C labels at Ala21 and Leu34 in Aβ_{1-42} fibrils (Figure 9b) and also inconsistent with solid-state NMR data on Aβ_{1-40} fibrils (*17*, *20*).

It must be emphasized that our solid-state NMR data do not imply that the entire Aβ_{10-35} or Aβ_{1-42} peptide backbone adopts a β-strand conformation in the amyloid fibrils, nor

do they prove the existence of in-register intermolecular *hydrogen bonding* (as opposed to in-register *alignment*) along the entire length of the peptide. In fact, approximately the first 10 residues at the N-terminal end of Aβ_{1-40} and Aβ_{1-42} appear structurally disordered in the fibrils, as indicated by solid-state NMR data (*17*, *20*, *21*) and by the observation of proteolytic digestion of these residues in vivo (*40*, *41*, *43*) and in vitro (*42*). In addition, solid-state NMR data on Aβ_{1-40} fibrils, including both ^{13}C chemical shifts and measurements of backbone ϕ and ψ torsion angles (*21*), indicate a non-β-strand backbone conformation in residues 23−29 in Aβ_{1-40} fibrils. Nonetheless, all solid-state NMR data support a parallel alignment of adjacent peptide chains, with interchain spacings of approximately 0.5 nm, along the entire structurally ordered regions of Aβ_{10-35}, Aβ_{1-40}, and Aβ_{1-42}. The tertiary structure adopted by these peptides in the amyloid fibrils may be due to the simple fact that an in-register parallel alignment maximizes hydrophobic contacts within a single cross-β unit (*17*, *18*, *20*).

Interpretation of Structural Constraints from Electron Microscopy. Although the secondary and tertiary structures of all Aβ fibrils appear very similar under the conditions examined in this work, the quaternary structures revealed by EM and STEM measurements differ significantly. Aβ_{10-35} fibrils prepared at pH 3.7 appear as single filaments with an apparently uniform diameter of 6.6 ± 0.6 nm in EM images. STEM measurements indicate a homogeneous MPL value equal to twice the MPL of a single cross-β unit. It should be noted that an Aβ_{10-35} molecule would be approximately 8.8 nm in length if the entire peptide adopted a fully extended β-strand conformation. Thus, the observed Aβ_{10-35} fibril diameter suggests a backbone conformation that includes a bend or other non-β-strand conformation. In contrast, Aβ_{10-35} fibrils prepared at pH 7.4 exhibit a periodic modulation in diameter between 5.5 ± 1.0 and 10.5 ± 1.0 nm. The minimum diameter is approximately equal to the diameter of pH 3.7 fibrils, while the maximum diameter is slightly greater than the length of a single Aβ_{10-35} molecule in a fully extended β-strand conformation. The smallest MPL values determined from STEM measurements are approximately four times the MPL of a single cross-β unit. These results suggest that the minimal pH 7.4 fibril is a twisted pair of pH 3.7 fibrils. The pH 3.7 fibrils may then be considered the protofilament of Aβ_{10-35} fibrils, with two protofilaments comprising a single pH 7.4 fibril. Higher apparent MPL values for Aβ_{10-35} fibrils prepared at pH 7.4 may arise from lateral association of fibrils.

EM images of Aβ_{1-42} fibrils prepared at pH 7.4 show a heterogeneity of morphology, with some fibrils exhibiting a uniform diameter of 6.0 ± 1.0 nm and others exhibiting a periodically modulated diameter ranging from a minimum of 6.0 ± 1.0 nm to a maximum of 12.5 ± 2.5 nm. The length of an Aβ_{1-42} molecule in a fully extended β-strand conformation would be approximately 14.3 nm. The length after subtraction of a 10-residue disordered segment at the N-terminus would be approximately 10.9 nm. These observations suggest that the secondary structure of fibrillized Aβ_{1-42} also includes non-β-strand conformations. MPL values determined from STEM images range primarily between the MPL of two cross-β units and the MPL of four cross-β units. It therefore appears that the quaternary structure of Aβ_{1-42} fibrils may be quite similar to that of Aβ_{10-35} fibrils, i.e., that the Aβ_{1-42} protofilament is constructed from two cross-β units and that fibrils with higher MPL are primarily pairs of protofilaments. Under the conditions of our experiments on Aβ_{1-42}, single protofilaments coexist with paired protofilaments as well as larger fibril bundles.

In the collection of MPL data for Figure 4e, an attempt was made to select fibrils that were single filaments, rather than pairs or higher order assemblies of filaments. For this reason, the histogram does not accurately indicate the ratio of the number of protofilaments to the number of fibrils with higher MPL. The absence of a pronounced peak at approximately 38 kDa/nm should not be interpreted as an absence of paired protofilaments.

Relation to Other Structural Studies of Aβ Fibrils. Aβ_{10-35} fibrils have been studied extensively by Lynn, Meredith, Botto, and co-workers (*13*−*16*), using solid-state NMR measurements, EM images, small-angle neutron scattering (SANS), enzymatic cross-linking, and chemical derivatization, especially attachment of poly(ethylene glycol) (PEG) chains at the C-terminus of the peptide (*66*−*68*). Solid-state NMR measurements using the DRAWS technique (*13*, *14*, *16*) to measure intermolecular ^{13}C−^{13}C dipole−dipole couplings strongly support an in-register parallel alignment of peptide chains within a cross-β unit in Aβ_{10-35} fibrils prepared at pH 7.4, spanning the sequence from Val12 through Leu34. DRAWS data on Aβ_{10-35}−PEG fibrils also support an in-register parallel alignment (*15*). The data of Lynn, Meredith, Botto, and co-workers on Aβ_{10-35} were the first solid-state NMR measurements to show that Aβ fibrils contain parallel β-sheets. Our solid-state NMR data on Aβ_{10-35} and Aβ_{1-42} fibrils presented above, as well as earlier MQ NMR and fpRFDR-CT data on Aβ_{1-40} fibrils (*17*, *20*), are in agreement with the work of Lynn, Meredith, Botto, and co-workers. The solid-state NMR data reported above extend this work by showing that the parallel β-sheet structure in Aβ_{10-35} fibrils is retained at pH 3.7, that the parallel organization persists over at least three successive peptide chains within a β-sheet, and that Aβ_{1-42} fibrils have the same parallel β-sheet organization. In general, our results substantiate the view that Aβ_{10-35} is a relevant model of full-length Aβ peptides.

IR spectra of full-length Aβ fibrils (*24*, *25*) and other Aβ fibrils (*23*), in particular the observation of a splitting of the amide I band into a stronger band at approximately 1630 cm^{-1} and a weaker band at approximately 1695 cm^{-1}, have been interpreted as support for antiparallel β-sheet structures. Although measurements on certain model peptides favor this interpretation (*69*), recent IR studies of proteins containing parallel β-sheets (*70*) and simulations of IR spectra (*71*) demonstrate that these features of the amide I band are not a unique signature of antiparallel β-sheets.

Solid-state NMR data on Aβ_{16-22} and Aβ_{34-42} fibrils indicate antiparallel β-sheet structures (*11*, *18*), demonstrating that amyloid fibrils can exhibit a diversity of tertiary structures. These two Aβ fragments contain the central and C-terminal hydrophobic segments of full-length Aβ, respectively. Apparently, the tertiary structure in amyloid fibrils is not uniquely determined by the amino acid sequence at the level of seven- or nine-residue segments. Because both Aβ_{16-22} and Aβ_{34-42} contain a single hydrophobic segment with a positively charged N-terminus and negatively charged C-terminus, hydrophobic contacts could be maximized in

either a parallel or an antiparallel structure, while electrostatic interactions would be expected to favor the antiparallel structure. Amyloid fibrils formed by all Aβ fragments examined by solid-state NMR to date exhibit tertiary structures that juxtapose the hydrophobic segments of neighboring peptide chains.

Analysis of SANS data on Aβ_{10-35}−PEG fibrils at pH 5.6 yields an estimated MPL value for the peptide component alone of 31−37 kDa/nm (*15*), corresponding to five or six cross-β units. Although the estimated MPL value from SANS data appears roughly consistent with the MPL histogram from STEM data on Aβ_{10-35} fibrils prepared at pH 7.4 (Figure 3d), which shows a peak in the MPL distribution at 30 kDa/nm, the interpretation of EM and SANS data on Aβ_{10-35}−PEG fibrils given by Burkoth et al. (*15*) suggests that Aβ_{10-35}−PEG fibrils represent Aβ_{10-35} protofilaments whose association into twisted-pair fibrils is blocked by the C-terminal PEG moieties. One might therefore expect the MPL value of the peptide component in Aβ_{10-35}−PEG fibrils to equal that of Aβ_{10-35} fibrils prepared at pH 3.7 (Figure 3c). This apparent discrepancy between STEM and SANS determinations of MPL remains to be resolved but may be due to differences in the pH values of the two measurements (*15*, *68*). It should be noted that the determination of MPL from STEM data is independent of any assumptions regarding the cross-sectional shape, diameter, or composition of the fibrils and is therefore a comparatively robust procedure.

Goldsbury et al. have reported a study of the time course of Aβ_{1-40} fibril formation at pH 7.4, using EM and STEM measurements (*54*). An MPL histogram for fibrils formed at an early stage (called "protofibrils" by Goldsbury et al.) shows a single peak at approximately 19 kDa/nm, corresponding to two cross-β units as in the Aβ_{10-35} and Aβ_{1-42} protofilaments discussed above. Higher MPL values appear at a later stage, corresponding primarily to between two and four β-sheet laminae and in good agreement with our data for Aβ_{1-42} fibrils (Figure 4e). We have also obtained STEM data on Aβ_{1-40} fibrils similar to those of Goldsbury et al. (data not shown). Thus, it appears that both Aβ_{1-40} and Aβ_{1-42} predominantly form fibrils with between one and two protofilaments at pH 7.4, with the protofilament consisting of two cross-β units, while Aβ_{10-35} predominantly forms fibrils with two or more protofilaments at pH 7.4.

Harper et al. have characterized Aβ_{1-40} and Aβ_{1-42} fibrils by AFM (*36*, *55*). Although the kinetics and concentration dependence of fibrillization differ, the structural features of Aβ_{1-40} and Aβ_{1-42} fibrils seen in AFM images are similar. AFM images of Aβ_{1-40} fibrils reveal the formation of twisted-pair fibrils, called "type 1 fibrils" by Harper et al. (*36*), from apparently single filaments. The single filaments in AFM images may correspond to the protofilaments comprised of two cross-β units discussed above. The type 1 fibrils exhibit periodic modulation in diameter (inferred from AFM tip height) between approximately 6 and approximately 9 nm and a periodicity of approximately 40 nm. These dimensions are in approximate, although not quantitative, agreement with the dimensions of apparently twisted fibrils in Figures 4 and 5.

Egnaczyk et al. have reported photoaffinity cross-linking experiments on Aβ_{1-40} in which a specific cross-link between side chains of Met35 and a L-*p*-benzoylphenylalanine residue substituted for Phe4 was identified and interpreted as evidence for antiparallel β-sheets in Aβ_{1-40} fibrils (*72*). The source of the apparent discrepancy between this photoaffinity cross-linking result and the tertiary structure revealed by solid-state NMR is not yet understood. The possibility exists that the reported cross-links form between different fibrils or between different β-sheets within a fibril, rather than within a single β-sheet. It should be noted that Phe4 is located in the disordered N-terminal segment of Aβ_{1-40}.

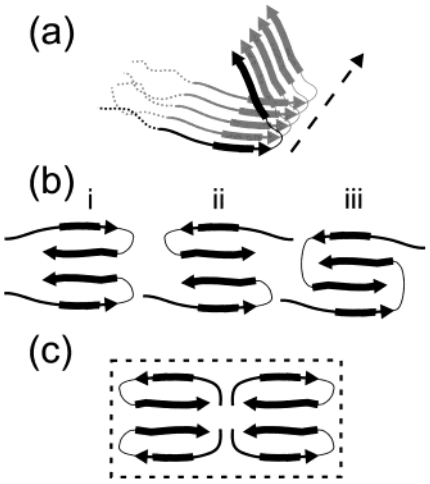

FIGURE 11: (a) Schematic model of a single cross-β unit in Aβ_{10-35} or Aβ_{1-42} fibrils consistent with solid-state NMR data. The fibrillized peptide contains two β-strand segments (lines ending in arrowheads) connected by a loop containing non-β-strand conformations (thinner lines). The central and C-terminal hydrophobic segments (thicker lines) are contained in the β-strands. Dotted lines represent the disordered N-terminal segment of Aβ_{1-42}. Neighboring peptide chains have an in-register parallel alignment. The dashed arrow indicates the long axis of the fibril. For clarity, the closest peptide molecule is in black and the others are in gray. (b) Cross sections of Aβ_{10-35} protofilaments constructed from two cross-β units, consistent with the EM and STEM data on pH 3.7 fibrils in Figures 2 and 3. The long axis of the protofilament is perpendicular to the page. Three possible models for the quaternary structure are shown. (c) Cross section of a possible Aβ_{10-35} fibril constructed from two protofilaments with structure i. The model is drawn approximately to scale, assuming the β-strand segments in each peptide molecule span residues 10−22 and 30−35. Hydrophobic segments are residues 17−21 and 29−35. The dashed rectangle is 5 nm × 10 nm, representing the approximate dimensions observed in EM images of twisted-pair Aβ_{10-35} fibrils at pH 7.4 in Figure 2.

Structural Model for Aβ Fibrils. Experimental data obtained to date are not sufficient to determine a unique, high-resolution structural model for Aβ fibrils. In particular, the precise limits on the β-strand segments in Aβ fibrils, the backbone conformation in intervening segments, the side chain conformations, and the correct quaternary contacts remain to be determined unequivocally. Nonetheless, as a means of clarifying the structural issues and summarizing the current state of knowledge, possible structural models for Aβ_{10-35} and Aβ_{1-42} fibrils are depicted schematically in Figure 11.

Figure 11a shows a model for the cross-β unit that is consistent with constraints on secondary and tertiary structure from solid-state NMR. In this model, residues 1−9 are structurally disordered (and absent in Aβ_{10-35}). Residues 10−22 (encompassing the hydrophobic segment spanning residues 17−21) and residues 30 through the C-terminus form β-strands. The two β-strand segments form in-register parallel β-sheets. Residues 23−29 form a loop or hinge between the two β-sheets (but not a true β-hairpin with intramolecular

hydrogen bonds between backbone atoms). We have recently reported NMR chemical shift and torsion angle data for Aβ_{1-40} fibrils that support the secondary structure depicted in Figure 11a (*21*).

Figure 11b shows three possible quaternary structures for an Aβ_{10-35} or Aβ_{1-42} protofilament constructed from two cross-β units. Other quaternary structures are possible, but these three are roughly consistent with the protofilament diameters observed in EM images and maximize the sequestration of hydrophobic residues from the surrounding aqueous medium in which the fibrils form.

Figure 11c shows one possible quaternary structure for Aβ_{10-35} fibrils constructed from two protofilaments. The model in Figure 11c is roughly consistent with the dimensions in EM images of fibrils with periodically modulated diameters due to an apparent twist (Figures 2c−f and 4a,b). This particular model is also consistent with the observed pH dependence of Aβ_{10-35} protofilament association (Figures 2 and 3), because potentially titratable Glu11, His13, and His14 residues are located in the interface between protofilaments. This model is also consistent with the observation that C-terminal PEG blocks protofilament association (*15*, *66*, *67*). A model similar to that in Figure 11c may also apply to Aβ_{1-42} fibrils, but with an extended C-terminal β-strand segment and with a conformation of the N-terminal β-strand that allows residues 1−9 to be located outside the structured core of the fibril.

Finally, the models in Figure 11 are variants of the laminated cross-β structure for amyloid fibrils that has been commonly invoked to account for X-ray diffraction (*9*, *56*, *57*) and EM (*6*) data. The fact that our STEM measurements indicate MPL values for Aβ protofilaments that are an integral multiple of the MPL of a single cross-β unit (Figure 3b and 4e) is consistent with, but does not prove, a laminated cross-β structure containing relatively little water or other nonpeptide material (less than 10 wt %). Nonlaminated structural models have also been proposed (*26*, *58*), reminiscent of the pectate lyase C (*73*) and P.69 pertactin (*74*) protein structures. Both EM (*75*) and diffraction (*53*) data have been interpreted as support for a tubular structure of Aβ fibrils. Additional experimental data, including additional solid-state NMR constraints on secondary and quaternary structure, may soon establish the full details of the structure of Aβ fibrils at the molecular level.

ACKNOWLEDGMENT

We thank Jennifer Reed for assistance with peptide synthesis and purification, Dr. L. K. Pannell for mass spectrometric measurements, and Nancy W. Rizzo for electron microscopy. Simulations of NMR data were executed on the SGI Origin 2000 computer in the National Institutes of Health Center for Information Technology. Development of solid-state NMR methodology was supported by the NIH Intramural AIDS Targeted Antiviral Program.

REFERENCES

1. Sunde, M., and Blake, C. C. F. (1998) *Q. Rev. Biophys. 31*, 1−39.
2. Sipe, J. D. (1992) *Annu. Rev. Biochem. 61*, 947−975.
3. Glenner, G. G., and Wong, C. W. (1984) *Biochem. Biophys. Res. Commun. 120*, 885−890.
4. Yankner, B. A. (1996) *Neuron 16*, 921−932.
5. Storey, E., and Cappai, R. (1999) *Neuropathol. Appl. Neurobiol. 25*, 81−97.
6. Jimenez, J. L., Guijarro, J. L., Orlova, E., Zurdo, J., Dobson, C. M., Sunde, M., and Saibil, H. R. (1999) *EMBO J. 18*, 815−821.
7. Chiti, F., Webster, P., Taddei, N., Clark, A., Stefani, M., Ramponi, G., and Dobson, C. M. (1999) *Proc. Natl. Acad. Sci. U.S.A. 96*, 3590−3594.
8. Inouye, H., Fraser, P. E., and Kirschner, D. A. (1993) *Biophys. J. 64*, 502−519.
9. Sunde, M., Serpell, L. C., Bartlam, M., Fraser, P. E., Pepys, M. B., and Blake, C. C. F. (1997) *J. Mol. Biol. 273*, 729−739.
10. Griffiths, J. M., Ashburn, T. T., Auger, M., Costa, P. R., Griffin, R. G., and Lansbury, P. T. (1995) *J. Am. Chem. Soc. 117*, 3539−3546.
11. Lansbury, P. T., Costa, P. R., Griffiths, J. M., Simon, E. J., Auger, M., Halverson, K. J., Kocisko, D. A., Hendsch, Z. S., Ashburn, T. T., Spencer, R. G. S., Tidor, B., and Griffin, R. G. (1995) *Nat. Struct. Biol. 2*, 990−998.
12. Costa, P. R., Kocisko, D. A., Sun, B. Q., Lansbury, P. T., and Griffin, R. G. (1997) *J. Am. Chem. Soc. 119*, 10487−10493.
13. Benzinger, T. L. S., Gregory, D. M., Burkoth, T. S., Miller-Auer, H., Lynn, D. G., Botto, R. E., and Meredith, S. C. (1998) *Proc. Natl. Acad. Sci. U.S.A. 95*, 13407−13412.
14. Gregory, D. M., Benzinger, T. L. S., Burkoth, T. S., Miller-Auer, H., Lynn, D. G., Meredith, S. C., and Botto, R. E. (1998) *Solid-State Nucl. Magn. Reson. 13*, 149−166.
15. Burkoth, T. S., Benzinger, T. L. S., Urban, V., Morgan, D. M., Gregory, D. M., Thiyagarajan, P., Botto, R. E., Meredith, S. C., and Lynn, D. G. (2000) *J. Am. Chem. Soc. 122*, 7883−7889.
16. Benzinger, T. L. S., Gregory, D. M., Burkoth, T. S., Miller-Auer, H., Lynn, D. G., Botto, R. E., and Meredith, S. C. (2000) *Biochemistry 39*, 3491−3499.
17. Antzutkin, O. N., Balbach, J. J., Leapman, R. D., Rizzo, N. W., Reed, J., and Tycko, R. (2000) *Proc. Natl. Acad. Sci. U.S.A. 97*, 13045−13050.
18. Balbach, J. J., Ishii, Y., Antzutkin, O. N., Leapman, R. D., Rizzo, N. W., Dyda, F., Reed, J., and Tycko, R. (2000) *Biochemistry 39*, 13748−13759.
19. Ishii, Y., Yesinowski, J. P., and Tycko, R. (2001) *J. Am. Chem. Soc. 123*, 2921−2922.
20. Balbach, J. J., Petkova, A. T., Oyler, N. A., Antzutkin, O. N., Gordon, D. G., Meredith, S. C., and Tycko, R. (2002) *Biophys. J. 83*, 1205−1216.
21. Petkova, A. T., Ishii, Y., Balbach, J. J., Antzutkin, O. N., Leapman, R. D., Delaglio, F., and Tycko, R. (2002) *Proc. Natl. Acad. Sci. U.S.A.* (in press).
22. Ishii, Y. (2001) *J. Chem. Phys. 114*, 8473−8483.
23. Fraser, P. E., McLachlan, D. R., Surewicz, W. K., Mizzen, C. A., Snow, A. D., Nguyen, J. T., and Kirschner, D. A. (1994) *J. Mol. Biol. 244*, 64−73.
24. Fraser, P. E., Nguyen, J. T., Inouye, H., Surewicz, W. K., Selkoe, D. J., Podlisny, M. B., and Kirschner, D. A. (1992) *Biochemistry 31*, 10716−10723.
25. Hilbich, C., Kisterswoike, B., Reed, J., Masters, C. L., and Beyreuther, K. (1991) *J. Mol. Biol. 218*, 149−163.
26. Lazo, N. D., and Downing, D. T. (1998) *Biochemistry 37*, 1731−1735.
27. Chaney, M. O., Webster, S. D., Kuo, Y. M., and Roher, A. E. (1998) *Protein Eng. 11*, 761−767.
28. Li, L. P., Darden, T. A., Bartolotti, L., Kominos, D., and Pedersen, L. G. (1999) *Biophys. J. 76*, 2871−2878.
29. Tjernberg, L. O., Callaway, D. J. E., Tjernberg, A., Hahne, S., Lilliehook, C., Terenius, L., Thyberg, J., and Nordstedt, C. (1999) *J. Biol. Chem. 274*, 12619−12625.
30. George, A. R., and Howlett, D. R. (1999) *Biopolymers 50*, 733−741.
31. Antzutkin, O. N., and Tycko, R. (1999) *J. Chem. Phys. 110*, 2749−2752.
32. Roher, A. E., Lowenson, J. D., Clarke, S., Woods, A. S., Cotter, R. J., Gowing, E., and Ball, M. J. (1993) *Proc. Natl. Acad. Sci. U.S.A. 90*, 10836−10840.
33. Iwatsubo, T., Odaka, A., Suzuki, N., Mizusawa, H., Nukina, N., and Ihara, Y. (1994) *Neuron 13*, 45−53.
34. Iwatsubo, T. (1999) *Acta Histochem. Cytochem. 32*, 13−15.
35. Jarrett, J. T., Berger, E. P., and Lansbury, P. T. (1993) *Biochemistry 32*, 4693−4697.
36. Harper, J. D., Wong, S. S., Lieber, C. M., and Lansbury, P. T. (1997) *Chem. Biol. 4*, 119−125.

37. Lee, J. P., Stimson, E. R., Ghilardi, J. R., Mantyh, P. W., Lu, Y. A., Felix, A. M., Llanos, W., Behbin, A., Cummings, M., Vancriekinge, M., Timms, W., and Maggio, J. E. (1995) *Biochemistry 34*, 5191−5200.
38. Esler, W. P., Stimson, E. R., Ghilardi, J. R., Lu, Y. A., Felix, A. M., Vinters, H. V., Mantyh, P. W., Lee, J. P., and Maggio, J. E. (1996) *Biochemistry 35*, 13914−13921.
39. Zhang, S., Iwata, K., Lachenmann, M. J., Peng, J. W., Li, S., Stimson, E. R., Lu, Y., Felix, A. M., Maggio, J. E., and Lee, J. P. (2000) *J. Struct. Biol. 130*, 130−141.
40. Roher, A. E., Lowenson, J. D., Clarke, S., Wolkow, C., Wang, R., Cotter, R. J., Reardon, I. M., Zurcherneely, H. A., Heinrikson, R. L., Ball, M. J., and Greenberg, B. D. (1993) *J. Biol. Chem. 268*, 3072−3083.
41. Saido, T. C., YamaoHarigaya, W., Iwatsubo, T., and Kawashima, S. (1996) *Neurosci. Lett. 215*, 173−176.
42. Kheterpal, I., Williams, A., Murphy, C., Bledsoe, B., and Wetzel, R. (2001) *Biochemistry 40*, 11757−11767.
43. Maxfield, F. R., personal communication.
44. Hilbich, C., Kisterswoike, B., Reed, J., Masters, C. L., and Beyreuther, K. (1992) *J. Mol. Biol. 228*, 460−473.
45. Wood, S. J., Wetzel, R., Martin, J. D., and Hurle, M. R. (1995) *Biochemistry 34*, 724−730.
46. Wall, J. S., and Hainfeld, J. F. (1986) *Annu. Rev. Biophys. Biophys. Chem. 15*, 355−376.
47. Tycko, R. (1999) *J. Magn. Reson. 139*, 302−307.
48. Suter, D., Liu, S. B., Baum, J., and Pines, A. (1987) *Chem. Phys. 114*, 103−109.
49. Ishii, Y., Balbach, J. J., and Tycko, R. (2001) *Chem. Phys. 266*, 231−236.
50. Anderson, R. C., Gullion, T., Joers, J. M., Shapiro, M., Villhauer, E. B., and Weber, H. P. (1995) *J. Am. Chem. Soc. 117*, 10546−10550.
51. Gullion, T., and Schaefer, J. (1989) *J. Magn. Reson. 81*, 196−200.
52. Petkova, A. T., and Tycko, R. (2002) *J. Magn. Reson. 155*, 293−299.
53. Malinchik, S. B., Inouye, H., Szumowski, K. E., and Kirschner, D. A. (1998) *Biophys. J. 74*, 537−545.
54. Goldsbury, C. S., Wirtz, S., Muller, S. A., Sunderji, S., Wicki, P., Aebi, U., and Frey, P. (2000) *J. Struct. Biol. 130*, 217−231.
55. Harper, J. D., Lieber, C. M., and Lansbury, P. T. (1997) *Chem. Biol. 4*, 951−959.
56. Serpell, L. C., Blake, C. C. F., and Fraser, P. E. (2000) *Biochemistry 39*, 13269−13275.
57. Blake, C., and Serpell, L. (1996) *Structure 4*, 989−998.
58. Perutz, M. F., Finch, J. T., Berriman, J., and Lesk, A. (2002) *Proc. Natl. Acad. Sci. U.S.A. 99*, 5591−5595.
59. Harper, J. D., Wong, S. S., Lieber, C. M., and Lansbury, P. T. (1999) *Biochemistry 38*, 8972−8980.
60. Saito, H. (1986) *Magn. Reson. Chem. 24*, 835−852.
61. Luca, S., Filippov, D. V., van Boom, J. H., Oschkinat, H., de Groot, H. J. M., and Baldus, M. (2001) *J. Biomol. NMR 20*, 325−331.
62. Wishart, D. S., Sykes, B. D., and Richards, F. M. (1991) *J. Mol. Biol. 222*, 311−333.
63. Spera, S., and Bax, A. (1991) *J. Am. Chem. Soc. 113*, 5490−5492.
64. Iwadate, M., Asakura, T., and Williamson, M. P. (1999) *J. Biomol. NMR 13*, 199−211.
65. Gregory, D. M., Mitchell, D. J., Stringer, J. A., Kiihne, S., Shiels, J. C., Callahan, J., Mehta, M. A., and Drobny, G. P. (1995) *Chem. Phys. Lett. 246*, 654−663.
66. Burkoth, T. S., Benzinger, T. L. S., Jones, D. N. M., Hallenga, K., Meredith, S. C., and Lynn, D. G. (1998) *J. Am. Chem. Soc. 120*, 7655−7656.
67. Burkoth, T. S., Benzinger, T. L. S., Urban, V., Lynn, D. G., Meredith, S. C., and Thiyagarajan, P. (1999) *J. Am. Chem. Soc. 121*, 7429−7430.
68. Thiyagarajan, P., Burkoth, T. S., Urban, V., Seifert, S., Benzinger, T. L. S., Morgan, D. M., Gordon, D., Meredith, S. C., and Lynn, D. G. (2000) *J. Appl. Crystallogr. 33*, 535−539.
69. Yamada, N., Ariga, K., Naito, M., Matsubara, K., and Koyama, E. (1998) *J. Am. Chem. Soc. 120*, 12192−12199.
70. Khurana, R., and Fink, A. L. (2000) *Biophys. J. 78*, 994−1000.
71. Kubelka, J., and Keiderling, T. A. (2001) *J. Am. Chem. Soc. 123*, 12048−12058.
72. Egnaczyk, G. F., Greis, K. D., Stimson, E. R., and Maggio, J. E. (2001) *Biochemistry 40*, 11706−11714.
73. Yoder, M. D., Keen, N. T., and Jurnak, F. (1993) *Science 260*, 1503−1507.
74. Emsley, P., Charles, I. G., Fairweather, N. F., and Isaacs, N. W. (1996) *Nature 381*, 90−92.
75. Serpell, L. C., and Smith, J. M. (2000) *J. Mol. Biol. 299*, 225−231.
76. Wishart, D. S., Bigam, C. G., Holm, A., Hodges, R. S., and Sykes, B. D. (1995) *J. Biomol. NMR 5*, 67−81.

BI0204185